SGG SGS sc | nat
Swiss Journal of Geosciences

ORIGINAL PAPER Open Access

Anatomy of a km-scale fault zone controlling the Oligo-Miocene bending of the Ligurian Alps (NW Italy): integration of field and 3D high-resolution digital outcrop model data

Ludovico Manna[1*], Michele Perozzo[1], Niccolò Menegoni[2], Silvia Tamburelli[1], Laura Crispini[3], Laura Federico[3], Silvio Seno[1] and Matteo Maino[1,4]

Abstract

We report the first description of a ~ 15 km long NE-SW-striking transtensive fault network crosscutting the metamorphic units of the Ligurian Alps. The main fault zone, hereby named *Horse Head Fault Zone*, is up to 250 m thick, involves quarzite, metarhyolite, marble and alternation of dolostone and limestone and minor pelite. Relatively narrow (~ 1–3 m-thick) fault cores are characterized by gouge and cataclasites, surrounded by brecciated damage zones as thick as tens to hundreds of meters. Damage zones show widespread evidence for dilation in the form of dilation breccia, large calcite crystals and aggregates, and centimeter- to meter-thick veins. Moreover, the fault zone contains a multitude of polished slip surfaces with multiple sets of slickensides and slickenfibers. Oblique to strike-slip kinematics dominates over the large part of the fault mirrors and both overprint and are overprinted by down-dip slip surfaces. The fault network includes dominant NE-SW right-lateral faults with a minor normal component and NW–SE left-lateral steep faults with a negligible reverse component, consistent with a km-size dextral NE-SW-striking Riedel shear zone, in turn representing an antithetic R′ of the regional sinistral shear zone constituted by the Ligurian Alps after the nappe stacking. The *Horse Head Fault Zone* accommodated km-scale displacement before the Early Miocene, as it is sealed by the sedimentary deposits of the Finale Ligure Basin, thus predating the Corsica-Sardinia drifting. Results of this work constraint the bending of the Ligurian Alps as part of the Western Alpine arc as accomplished through two consecutive, late Oligocene and Early Miocene, stages driven by the combination of Adria rotation and the rollback of the Apennine subduction.

Keywords Fault zone, Digital outcrop model, Riedel shears, Ligurian Alps, Liguro-provençal basin, Corsica-sardinia drifting, Adria rotation, Apennine subduction

Editorial handling: Salvatore Iaccarino.

*Correspondence:
Ludovico Manna
ludovico.manna01@universitadipavia.it
Full list of author information is available at the end of the article

1 Introduction

We present the first description of a large fault zone in the Ligurian Alps in front of the northern margin of the Liguro-Provençal basin. It is a NE-SW striking network of faults, reaching ~ 15 km in length and up to 250 m in width. The fault zone was recognized during the survey conducted in the framework of the Italian geological mapping project (CARG, Sheet 245—Albenga) and in the following we refer to it as *Horse Head Fault zone* from a peculiar morphology emerging on one main slip surface (Fig. 1B). The newly discovered large fault provides significant new constraints for the interpretation of the geometry and kinematics of the post-metamorphic fault network of the Ligurian Alps. The *Horse Head Fault zone* runs parallel to the northern margin of the Liguro-Provençal Basin (Figs. 1, 2), which opened since the Oligocene in response to the Alpine collision, the eastward Apennine migration and the Corsica-Sardinia drifting (Jolivet and Faccenna, 2000; Rosenbaum and Lister, 2004). The Ligurian Alps, as the southernmost termination of the Western Alpine arc, accommodated these movements through an anticlockwise rotation up to ~ 120° (Collombet et al., 2002), whereas the underlying post-collisional sediments of the Tertiary Piedmont Basin (TPB) record only a ~ 50° rotation (Maffione et al., 2008) (Figs. 1A, 2). The reason of such discrepancy is debated, as it is interpreted as due to either two stages (the first one involving only Alpine metamorphic rocks, the second also TPB rocks) or local rotation (e.g. Collombet et al., 2002; Maffione et al., 2008). This ambiguity compromises the understanding of the role of Adria rotation and the rollback of the Apenninic slab in shaping the Alpine curvature (Schmid and Kissling, 2000; Handy et al., 2010; 2021; Vignaroli et al., 2010; Kästle et al., 2020; Ring et al., 2022).

Defining the geometry, the kinematic and the timing of the main structures that assisted the bending of the Ligurian belt is a key issue to improve our understanding of the Alpine evolution. In this paper, we report and describe the meso-scale deformation pattern of a new large fault zone and interpret its timing in relation with the syn- to post-orogenic structures and the sedimentary record. We propose for this fault zone a major role in controlling the Oligocene–Miocene tectonic evolution of the Ligurian pivot.

We address the structural investigation integrating traditional field surveying methods with Digital Outcrop Models (DOMs). Traditional surveying allows characterizing only small and accessible outcrop portions, whereas photogrammetry may perform high-resolution DOMs of large (and even inaccessible) areas supporting the collection of large dataset (Bellian et al., 2005; McCaffrey et al., 2005; Westoby et al., 2012; Menegoni et al., 2019). The use of Unmanned Aerial Vehicles (UAVs) applied to Digital Photogrammetry (UAV-DP) provides high-quality outcrop models from meter to kilometer scale, allowing for accurate multiscale structural analysis (Cawood et al., 2017). However, mm-scale details, such as the steps associated with slickolites and slickenfibers, have yet to be physically verified on the rock. Human observation on the outcrop-scale structural investigation is still essential for such an evaluation of complex geometries and multiple kinematics. Structural findings on the investigated new fault zone highlight that the fault rocks are

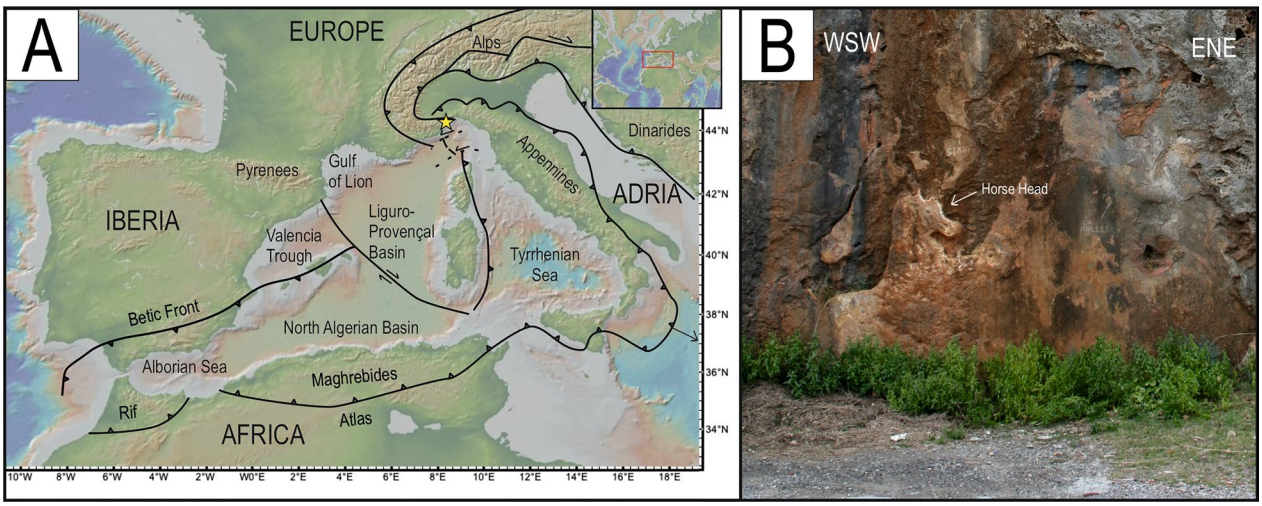

Fig. 1 **A** Simplified structural map of the West Mediterranean area. Yellow star indicates the study area within the Ligurian Alps (Fig. 2B). **B** Outcrop close to the Boissano village (Latitude 44.132299, Longitude 8.211948) of one of the main polished slip surfaces of the fault network with the peculiar horse head (white arrow) morphology that gives the name to the fault

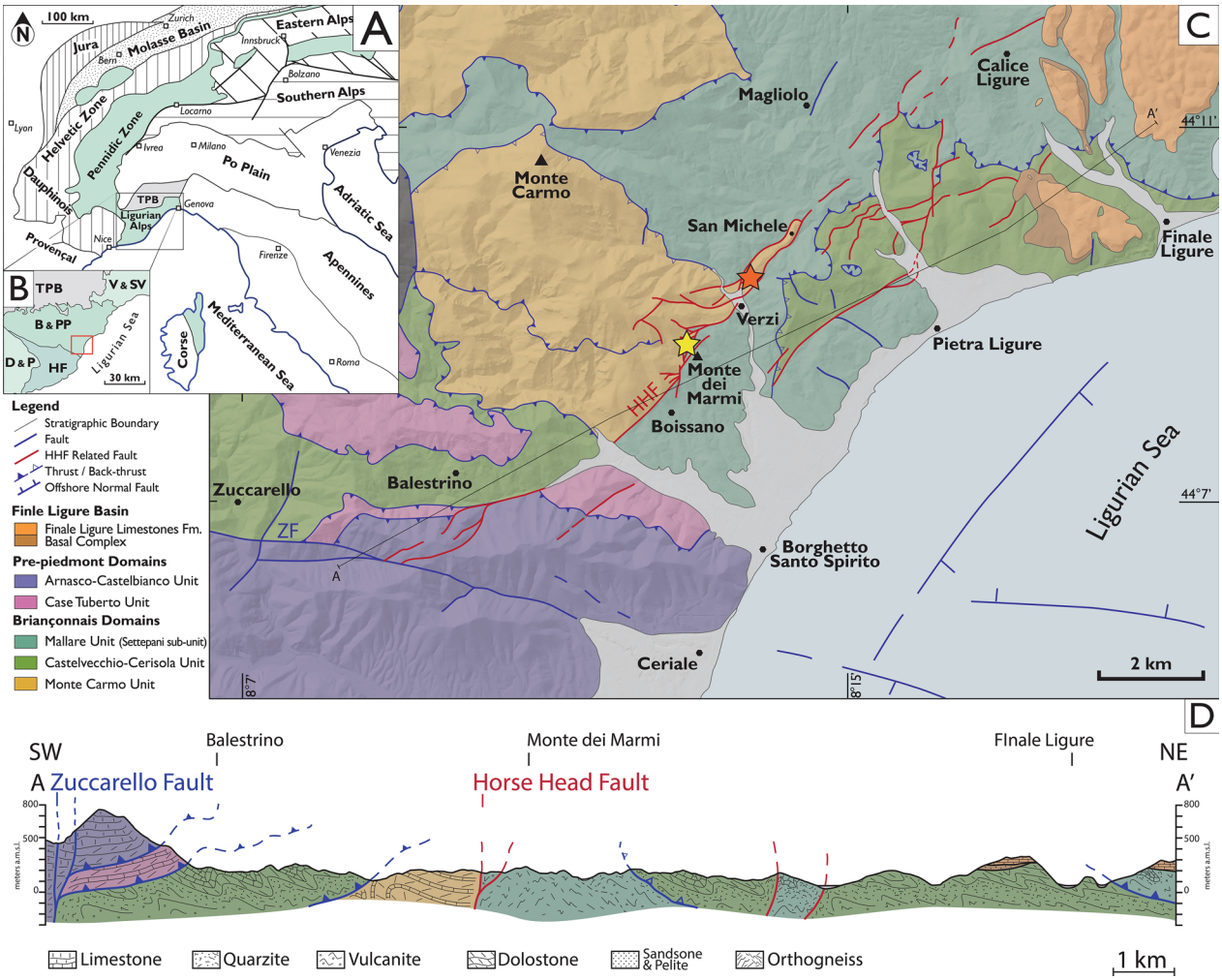

Fig. 2 **A** Tectonic sketch of the Alps (modified from Schmid, 2004). **B** Zoom of the main paleogeographic domains of the Ligurian Alps (from Bonini et al., 2010). **C** Simplified structural map of the Ligurian Alps between Finale Ligure and Ceriale (Liguria, NW Italy). *HHF* Horse Head Fault zone, *ZF* Zuccarello Fault zone. The study areas are indicated with orange and yellow marks (Respectively, Verzi and Monte dei Marmi). Offshore faults are derived from Morelli et al. (2022). A-A' indicates the trace of the geological cross-section. **D** Geological cross-section through the study area

characterized by multiphase switches among compressive-, extensional- and strike-slip-dominated regimes. Deciphering the deformation evolution of such a complex fault zone is a tectonic challenge. Heterogeneities from mechanical anisotropies and variations in lithology, depths of burial, metamorphism, fluid availability, orientation of stress field and so on (e.g. Fossen et al., 2019; Maino et al., 2021), concur to mix the deformation outputs, making hard the reconstruction of the step-by-step evolution. Furthermore, deformation may evolve progressively or through distinct deformation phases separated by periods of tectonic quiescence. A robust deformation history requires the reconstruction of the overprinting relationships correlated with the variations of kinematics and rheological behavior through time. We present a structural investigation aiming to combine the mm-scale details with a large amount of structural data in order to merge accuracy and statistically sounding analysis.

2 Background

2.1 Tectonic setting

The Ligurian region in NW Italy records a complex geological history comprising several rifting and orogenic phases that developed since the Cambrian up to now, as it still represents a tectonically active margin (e.g. Vanossi et al., 1984; 1994; Larroque et al., 2011; Soulet et al., 2016; Maino et al., 2013; 2019; Mueller et al., 2020; Morelli et al., 2022; Fig. 2). During the Cenozoic evolution of the central Mediterranean, the Ligurian region represented

the knot pivoting the opposite movements of the Alps and Apennines orogenic systems (e.g. Laubascher et al., 1992; Vanossi et al., 1994; Rosenbaum et al., 2002; Vignaroli et al., 2008; Crispini et al., 2009; Molli et al., 2010; Mosca et al., 2010; Maino et al., 2013; Schmid et al., 2017). Such divergent motion resulted from the oblique NW-directed Adria-Europe collision and the eastward migration of the Apennine arcs (Faccenna et al., 2004; Handy et al., 2010; Le Breton et al., 2021).

Since the Eocene, nappe stacking, folding and heterogeneous metamorphism (from eclogite to epizone) resulted from the convergence between Adria and Europe and the subduction of the interposed Ligurian-Piedmont Ocean (Trümpy, 1960; Dewey et al., 1989). Since the early Oligocene transition between the subduction and collision phases, the counterclockwise rotation of Adria has a major role in determining the present day structure of the Alps (Dewey et al., 1989; Platt et al., 1989; Laubascher, 1992; Ford et al., 2006; Ring and Gerdes, 2016). The Adria indentation and rotation beneath the Europe is thought to have promoted the right-lateral motion in the Western and Central Alps (e.g. Insubric Line, Simplon-Rhone Line, Pennine Basal Thrust, Briançonnais Front, Strura and Preit Lines), as well as the tightening and arcuate shape of the Western Alps (Mancktelow, 1992; Giglia et al., 1996; Schmid et al., 1996; 2004; Sue and Tricart, 2003; Handy et al., 2010; Champagnac et al., 2006; Malusà et al., 2009; Campani et al., 2010; Perrone et al., 2011; Campani et al., 2014; Cardello et al., 2016; Ring et al., 2022).

However, a major role in modifying the post-Oligocene structure of the Alps is also attributed to the evolution of the coeval Apennines–Maghrebides subduction (e.g. Malinverno and Ryan, 1986; Doglioni, 1991; Jolivet and Faccenna, 2000; Maffione et al., 2008; Fig. 1A). The retreat of the slab resulted in a progressive trench rotation from a NE-SW direction (i.e., parallel to the European passive margin) to a N-S trending (e.g. Carminati et al., 2012). This geodynamic process drove the eastward Apennines nappe stacking and migration (Castellarin, 2001). In the Northern Apennine, such rotation was accommodated by curvilinear thrusts and strike-slip faults (e.g. Villavernia-Varzi Faults, Ottone-Levanto Fault; Marroni et al., 2009; 2019).

The rollback of this west Mediterranean subduction zone caused the opening of several Oligo-Pliocene back-arc basins (i.e. the Alboran sea, Algerian basin, Valencia Trough, Liguro-Provençal basin, Thyrrenian sea; Rollet et al., 2002; Rosenbaum and Lister, 2004; Faccenna et al., 2004; Jolivet and Faccenna, 2000; Carminati et al., 2012; Fig. 1A).

The inception of the Ligurian-Provençal basin is documented by the volcanic record at ca. 32–30 Ma, above the previously thickened continental European crust (De Voogd et al., 1991; Séranne, 1999; Réhault et al., 2012 and references within). The oceanic spreading associated with the Liguro-Provençal opening is dated between ~ 22 and 15 Ma (Carminati et al., 1998; Speranza et al., 2002; Siravo et al., 2023) coeval with the drifting of the Corsica-Sardinia block (Rosenbaum et al., 2002; Rosenbaum and Lister, 2004; Gattacceca et al., 2007; Maffione et al., 2008; Maino et al., 2013; van Hinsbergen et al., 2014). In the Late Miocene-Quaternary, the Appenines back-arc extension switched to the Tyrrhenian Sea spreading (Patacca et al., 1990; Jolivet and Faccenna 2000), while the Ligurian Alps experienced uplift (Foeken et al., 2003; Larroque et al., 2009; Morelli et al., 2022).

2.2 Structure and stratigraphy of the study area

The investigated portion of the Ligurian Alps shows a stack of tectonic units (Monte Carmo, Mallare and Arnasco-Castelbianco; Fig. 2C) pertaining to the Briançonnais and Prepiedmont domains, which, in the Mesozoic times, were part of the European continental margin in front of the Piedmont-Ligurian oceanic realm (Fig. 2B, C); e.g. Vanossi et al., 1984; Bonini et al., 2010; Mueller et al., 2020). Briançonnais and Prepiedmont units are ideally constituted by a Palaeozoic basement (Maino et al., 2012, 2019), a Permian volcano-sedimentary succession (Dallagiovanna et al., 2009) and a more or less complete Meso-Cenozoic cover (Decarlis and Lualdi, 2011; Decarlis et al., 2013; Maino and Seno, 2016). The studied fault zone involves orthogneiss, metarhyolite and Triassic to Jurassic quartzite, dolostone, limestone and marble (Fig. 3).

As a consequence of the Alpine subduction and collision, the Briançonnais and Prepiedmont units experienced heterogeneous metamorphism from epizone to blueschists (Goffè and Bousquet, 2004; Seno et al., 2005; Maino et al., 2012). All investigated units followed a common deformation history, comprising two main Eocene ductile deformational phases (D1-2) with opposite tectonic vergence (SW and NE, respectively, associated with folding and backthrusting (Bonini et al., 2010; Maino et al., 2015a, b; 2020). A third ductile deformation phases (D3) produced large amplitude, open, upright folding characterizing the final exhumation of the deep-seated rocks after collision, constrained in the earliest Rupelian (35–32 Ma; Maino et al., 2012a; 2015a, b). While the syn-collisional structures of the study area are well-described in literature, a few post-metamorphic faults are reported only in the 1:100′000 scale geological map (Servizio Geologico d'Italia, 1971).

In the study area, since the Oligocene, a carbonate-siliciclastic coastal wedge sedimented in the Finale Ligure Basin, unconformably covered part of the Alpine

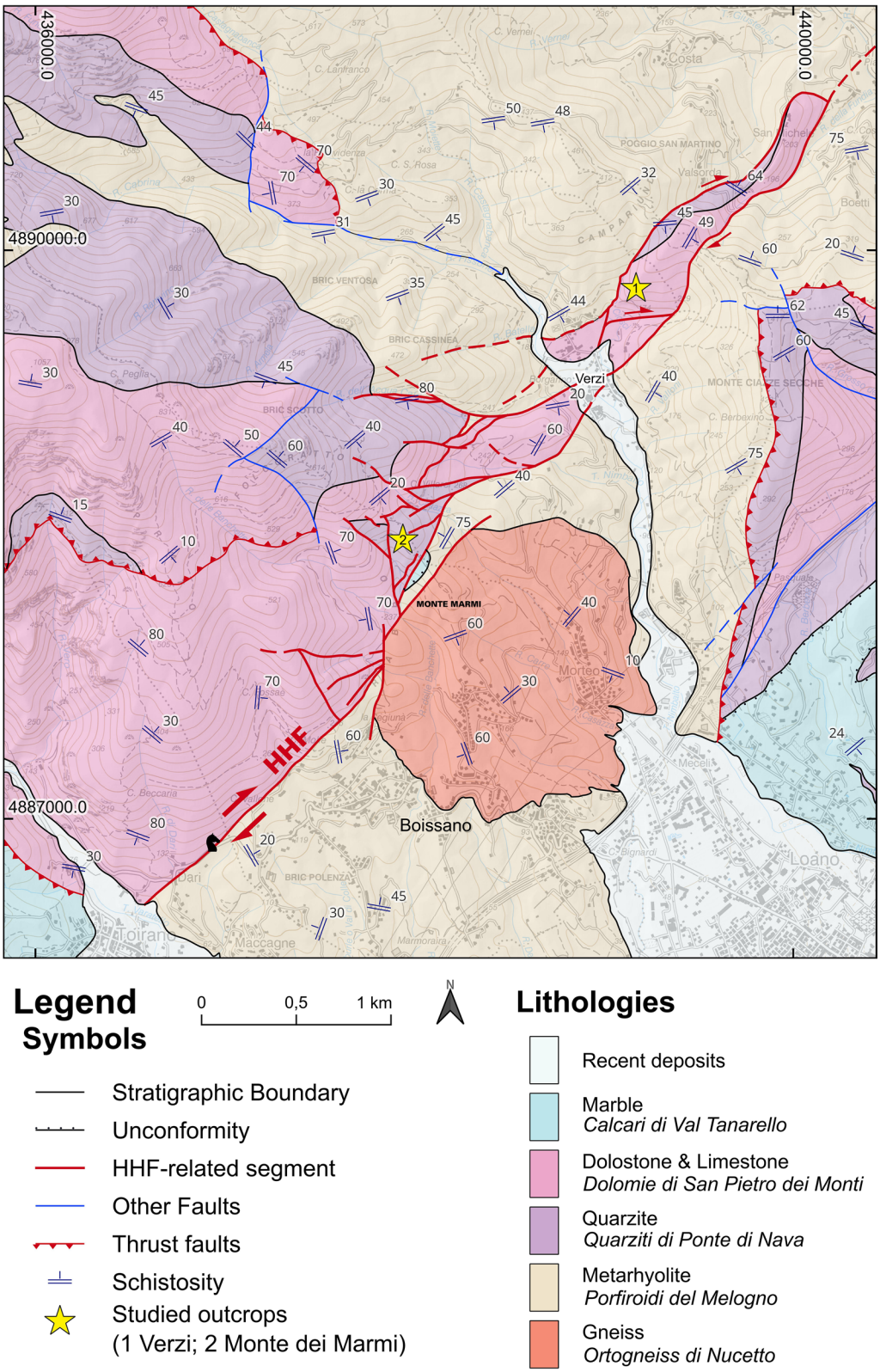

Fig. 3 Lithostratigraphic map of the main segment of the HHF zone. The field data were collected in the framework of the CARG project (Sheet 245–Albenga). Location of the fault mirror shown in Fig. 1B is indicated by the horse head symbol

metamorphic units (Fig. 2C; Boni et al., 1968; Brandano et al., 2015; Della Porta et al., 2022). Sedimentation started with a 10 to ~ 100 m thick, undated breccia followed by sands, conglomerates and marls with Aquitanian to Burdigalian age (Basal Complex of Finale Ligure Limestone Fm; Boni et al., 1968; Dallagiovanna et al., 2011). Up section, a ~ 250 m thick succession of Langhian to Serravallian bioclastic limestone constitutes the Finale Ligure Limestone Fm (Boni et al., 1968; Dallagiovanna et al., 2011; Brandano et al., 2015; Dalla Porta et al., 2022). Due to the lack of deformation evidence—including faulting—it is traditionally considered as a low-strain domain (Boni et al., 1968; Dallagiovanna et al., 2011; Dalla Porta et al., 2022). However, recently Mueller et al. (2023) discovered and described co-seismic deformations in the shallow sediments (a mix of cm- to m- size soft sediment deformation structures, clastic dikes and shear bands) allowing to constrain multiple seismic input in the Langhian-Serravallian times, coeval with the oceanic spreading of the Liguro-Provençal basin and the Corsica-Sardinia drifting.

North of the study area, the sediments of the TPB started to cover the metamorphic rocks of the Ligurian Alps in the early Oligocene (Fig. 2B; Gelati et al., 1998; Dallagiovanna et al., 2010). During the Oligocene–Miocene, the TPB accumulated a sedimentary succession up to ~ 4 km thick that recorded multistage deformation. A first Rupelian–early Chattian stage of extension driven by NW-directed faults was followed by a late Chattian drowning of the basin controlled by transtensional NE- to ENE-striking faults (Maino et al., 2013; Federico et al., 2020). In the Early Miocene, minor evidences of locally developed transpressive tectonics are documented in the basin (Carrapa et al., 2003; Crispini et al., 2009; Federico et al., 2014; Maino et al., 2013).

After the Messinian salinity crisis, incision of valley along the Ligurian paleo-coast occurred, while during the earliest Pliocene the river valleys were flooded by the sea and transformed into a series of coastal embayment filled by large Gilbert-type deltas (Boni et al., 1985; Clauzon et al., 1995). The heterogeneous fine- (Ortovero mudstone Fm) and coarse-grained (Monte Villa conglomerate Fm) facies and the depositional architecture of the infilling sequences outline a complex interaction between eustatic sea-level variation and tectonic activity. The depositional setting is described as resulting from the interaction of fast sea-level rise and steep-gradient shelf developed between the uplifting Alpine hinterland and the subsiding Ligurian basin under an extensional regime (Boni et al., 1985; Marini 2000; Foeken et al., 2003; Breda et al., 2007; 2009). Offshore, Pliocene–Pleistocene compressional reactivation of older extensional structures is well documented by the WSW–ENE-elongated Imperia Promontory and the subparallel intra-slope basin along the Ligurian margin (Chaumillon et al., 1994; Eva and Solarino, 1998; Calais et al., 2001; Larroque et al., 2011; Morelli et al., 2022). The focal mechanisms of the present-day earthquakes reveal a dominant transpressional regime (Eva and Solarino, 1998; Calais et al., 2001; Larroque et al., 2011; Morelli et al., 2022).

2.3 Rotation of the Ligurian Alps

The Ligurian Alps record the most prominent bending of the Western Alpine arc, which is outlined by the inversion of about 180°of the orogen around a vertical axis (Figs. 1A, 2A). Paleomagnetic data from the Western Alps, including the Ligurian segment, recognized a southward increasing counterclockwise rotation, from ~ 47 to ~ 117° (Thomas et al., 1999; Collombet et al., 2002). Such rotation is constrained as occurred after the main ductile deformation and metamorphic phases, therefore since the late Rupelian times (Maino et al., 2012; 2015a, b; Amadori et al., 2023). Further paleomagnetic investigation, instead, reveals that the TPB rotated ~ 50° counterclockwise in Early-Middle Miocene, whereas both Ligurian Alps and TPB have undergone no paleomagnetic rotation since the Late Miocene times. It remains unclear if the Ligurian Alps experienced rotation with different timing (Oligocene plus Miocene) and geodynamics with respect to the TPB (only Miocene), or the whole Western Alps rotated by ~ 50° in early Miocene and the Liguria underwent an additional local ~ 70° counterclockwise rotation.

The rotation mechanism causing the tightening of the Western Alpine arc is interpreted as driven by either (i) Adria rotation causing dextral faulting in the Central alps and left-lateral shear of the southern Western Alps or, (ii) nappe stacking of the Alpine wedge underlying the TPB that rotated along with Corsica-Sardinia in response to the rollback of the Apenninic slab (Schmid and Kissling, 2000; Collombet et al., 2002; Maffione et al., 2008; Vignaroli et al., 2008; Pleuger et al., 2012; Ring and Gerdes, 2016; Kästle, 2020). However, the paleomagnetic data are insufficient to discriminate between the possible mechanisms, mainly because of the poor recognition and understanding of the structures leading the rotation.

3 Methods

In this study, we present a structural analysis that integrates the structural field survey with the Unmanned Aerial Vehicle (UAV)-based Digital Outcrop Model. The field dataset was compiled during extensive mapping at the 1:5′000 scale, in the framework of the Italian geological mapping CARG project (CARG "Foglio 245-Albenga"; https://www.isprambiente.gov.it/Media/carg/). Fieldwork was performed at the outcrop scale, aimed at

investigating individual contacts between lithologies and tectonic structures, including folds, thrusts and faults. Faults recognized in the field have been characterized in terms of geometry, distribution of damage, type and composition of fault rocks and kinematics (Woodcock and Mort, 2008). We carried out UAV-based Digital Outcrop Model on the largest outcrop of faulted rocks (lat. 44.157870N, long. 8.238764), i.e. an abandoned quarry where a complex faults network is well exposed, because it has a scarce and dangerous accessibility and with the aim to collect statistically significant data.

3.1 Structural field analysis

The structural field survey was conducted by compass-clinometer measuring the orientation of faults and fractures. In this study, we refer to fracture as fault when the morphology or kinematic indicators are clearly visible. For what concerns the faults, the availability of various types of carbonate slickenfibers allowed us to measure the rake and sense of the fault slip vector. The acquired fault slip dataset was then analyzed using the software FaultKin 8 (Marrett and Allmendiger, 1990; Allmendiger et al., 2011). The dataset of the fracture orientation was analyzed using the software Stereonet 11 (Allmendiger et al., 2011).

3.2 UAV photogrammetric survey and digital outcrop model development and analysis

The UAV photogrammetric survey was conducted in November 2022 in the abandoned quarry close to Verzi village (Fig. 2) using a DJI Phantom 4 RTK (P4RTK) quadcopter, equipped by a 20 Megapixel camera and a Real Time Kinematic-Global Navigation Satellite System (RTK-GNSS), following the procedure described in Menegoni et al., (2022a). In Table. 1 the quadcopter specification are described.

Due to the near vertical attitude and complex geometry of the study outcrop we performed the UAV flights and photo capturing manually using a variable camera pitch, ranging from 85° (near horizontal camera view) to 65° (gently inclined camera view, around 30°), and a mixture of strips and independent/convergent acquisition models (Menegoni et al., 2018). Three different acquisition missions were performed in order to acquire three photogrammetric datasets of different image resolution (Fig. 4): DOM1, 7.07 mm/pixel; DOM2, 2.79 mm/pixel; DOM3, 1.22 mm/pixel. The specification of the UAV-photogrammetric missions are reported in Table. 2.

The possibility to combine the P4RTK with the DJI D-RTK 2 GNSS antenna allowed us to use the RTK-positioning setting. Using it, the P4RTK works as RTK-GNSS rover antenna and the DJI D-RTK 2 as RTK-GNSS base station and, therefore, it is possible to measure the camera capture positions with high accuracy (< 1.5 cm according manufacturer). In this study, we did not use Ground Control Points (GCPs) because for the study aims a high relative accuracy (DOM orientation and scale) is needed, whereas a high absolute accuracy (DOM positioning) was unnecessary. Menegoni et al. (2019) and (2020) show that a correct UAV photogrammetric survey executed without GCPs can achieve a high relative accuracy with errors in orientation and scale lower than 1° and 0.05%, respectively. Moreover, several studies (Peppa et al., 2019; Taddia et al., 2019; Stott et al., 2020; Štroner et al., 2020; Taddia et al., 2020) show that using the quadcopter P4RTK, together with the D-RTK2 GNSS base station, it is possible to obtain absolute accuracies lower than 7 cm that is considered largely acceptable for the aims of this study. The UAV imagery dataset was then used to process with the Metashape software Agisoft (2019) to obtain the DOMs (Fig. 4). The processing was performed following the procedures described in Inama et al. (2020) and using the image full resolution. The DOMs were then analysed following the procedure described in Panara et al. (2022a) and Menegoni et al. (2022b). It consists in the use of the open-source software CloudCompare (CloudCompare, 2019) and its tools and plugins for the spatial measurements. In particular, to perform the fault orientation and slip vector digital analysis we used the Plane tool and Lineation tool of the Compass plugin (Thiele et al., 2022). The Digital Fault (DF) data were then analyzed as the Field Fault (FF) data through the use the software FaultKin 8 (Marrett and Allmendiger, 1990; Allmendiger et al., 2011).

Table 1 Specification of the UAV used to perform the Digital Photogrammetric survey

Type	DJI Phantom 4 RTK
Weight (payload included)	1391 g
Camera sensor type	CMOS
Camera sensor size	1 inch
Camera sensor resolution	20 megapixels
Camera focal length	8.8 mm (35 mm format equivalent: 24 mm)
Camera shutter	Mechanical
Gimbal type	Mechanical 3-axis
Inertial Measurements Unit (IMU) accuracy	< 2°
GNSS type	Real time kinematic (RTK)
GNSS accuracy	< 1.5 cm

3.3 Fault-slip data inversion

Inversion of fault-slip data is meant to reconstruct the orientation of the local stress field from the study of the kinematics of an array of faults (e.g. Angelier 1989, 1990;

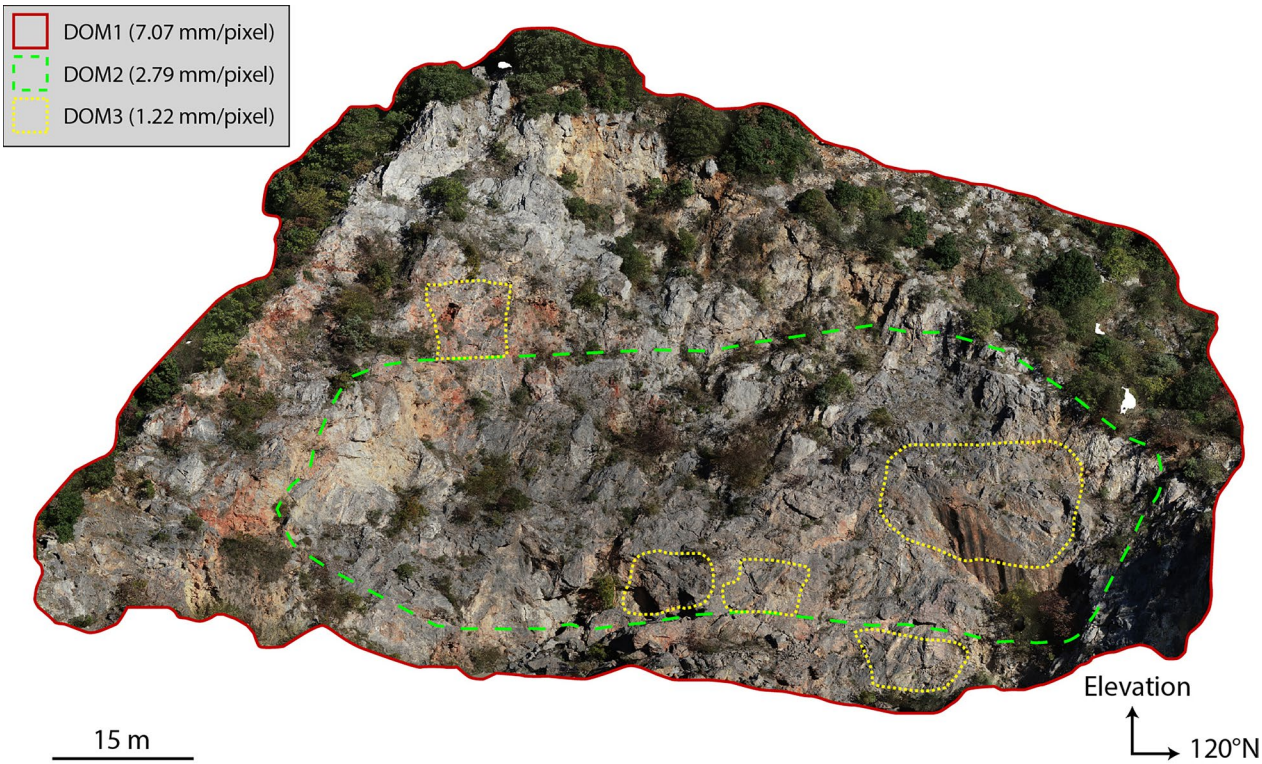

Fig. 4 Horizontal and orthographic view (view direction is 30°N) of DOM1 (abandoned quarry close to Verzi, lat. 44.157870N, long. 8.238764) where the areas covered by the DOMs with higher resolution (DOM2 and DOM3) are marked

Table 2 Specification of the different aerial-photogrammetric surveys

UAV type	Flight mode	Number of flights	Camera pitch	Mean camera—terrain distance	Mean resolution	Number of photos
DOM1	Manual	2	65–85°	30.20 m	7.07 mm/pixel	664
DOM2	Manual	1	84–90°	11.10 m	2.79 mm/pixel	379
DOM3	Manual	1	81–90°	4.79 m	1.22 mm/pixel	225

Delvaux and Sperner, 2003; Vanik et al., 2018). The first assumption of this method is that all the fault surfaces in the analyzed system formed under the same stress field. Other authors (e.g. Marrett and Allmendinger, 1990; Twiss and Unruh, 1998; Marrett and Peacock, 1999) claim that the result from the inversion are the axes of the incremental strain tensor and not the principal axes of stress. Actually, strain is related to stress by a constitutive relation that depends on the rheological behavior of the medium. The principal stress and strain axes are parallel only if the medium is isotropic, that is only if the two quantities are linearly dependent. In the following, this assumptions holds, and we will refer in the text to the directions of the principal strain axes.

The software that we used to perform fault-slip data inversion is Faultkin 8. It determines graphically the directions of the principal strain axes that correspond to the input fault-slip data (Marrett and Allmendinger, 1990; Allmendinger et al., 2011). The software uses the dynamic "P & T Dihedra Method" and the kinematic "P" (shortening) and "T" (extension) axes. The directions of the principal strain axes are calculated through the Bingham linked statistical distribution (Angelier and Mechler, 1977; Angelier 1990). Faultkin 8 allows to visualize the data on the directions of principal strains using the Bingham linked statistic to find the fault plane solution and plotting it on a stereonet. On the stereonets, the compressional domain is white-colored, while the extensional domain is in grey. Also the directions of the

strain axes are visualized on the plot with small squared dots of different colors. In the following, blue is the color of the dots representing the first strain axis, yellow is for the dots representing the intermediate axis and red for the dots of the minor strain axis, which are numbered 1,2 and 3, respectively.

4 Results

4.1 Fault architecture

The Horse Head Fault zone is a NE-SW ~ 15 km-long fault network encompassing a number of variably oriented fault segments, with lengths varying from a few tens of meters up to ~ 5 km (Fig. 2C). Fault zones developed across the tectonic units of Monte Carmo, Castelvecchio-Cerisola, Mallare, Case Tuberto and Arnasco-Castelbianco (Fig. 2C) representing also a major tectonic boundary among the units. The nappe pile changes its architecture across the two sides of the main fault, but the absence of clear stratigraphic or structural correlations prevents the determination of the real fault displacement. Along the major lineament, the SE termination of the Monte Carmo unit shrinks toward east showing horsetail geometry (Figs. 2C, 3). Horsetail terminations are also common along minor fault zones. The multiple folding and thrusting experienced by the rocks makes the determination of accurate fault displacement even along the minor fault segments difficult. However, cartographic reconstruction allows inferring vertical and horizontal displacement in the order of 10–300 m along secondary fault segments (Figs. 2C, 3). Collectively, azimuthal Gaussian distribution statistical analysis of the fault zones indicates one main peak at 50°E.

The studied fault network stops westward against a ~ 15 km-long, roughly E-W striking fault ("Zuccarello Fault"; Fig. 2C), for which a right-lateral transpressive kinematic postdating normal slip has been inferred (Vanossi, 1991). Eastward, the deposits of the Finale Ligure Basin unconformably overlain the faulted rock in the footwall (Fig. 2C).

The main fault zone reaches up to 250 m in thickness and tends to decrease towards the NE where it disappears below the Finale Ligure Basin deposits. The other km-long faults show thickness up to 50 m, whereas minor fault segments (< 1 km) are characterized by cm- to a few meter wide fault zone.

4.2 Fault zone structure

The principal fault zone of the *Horse Head Fault zone* network encompasses several lithologies, including dolostone, limestone, marble, quartzite and metarhyolite

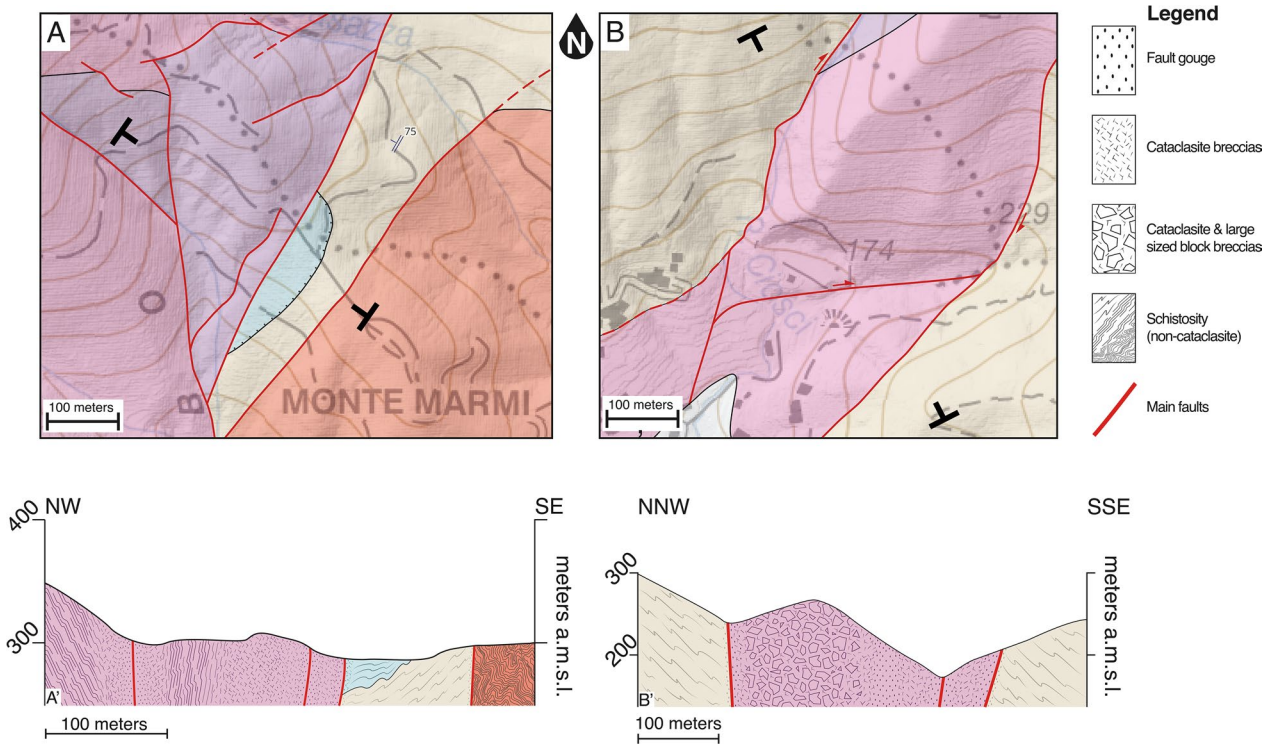

Fig. 5 Detailed geological maps and related cross-sections crossing the HHF zone at Outcrop 1-Verzi (**A**) and Outcrop 2-Monte dei Marmi (**B**). Refer to Fig. 3 for the location of the outcrops and the lithology colors

(Fig. 3). Here, we describe two well-exposed outcrops where the fault zone couples dolostone-metarhyolite and quartzite-dolostone-marble, respectively (Figs. 3 and 5).

4.2.1 Outcrop 1 (verzi quarry)

The first outcrop occurs in an abandoned quarry close to Verzi village (Figs. 2C, 3, 5A). Here the fault is structured as a 3 m-thick gouge in the core surrounded by a large, 150–250 m thick, damage zone (Figs. 5A, 6A). Damage zone mostly developed within mainly carbonate rocks (alternation of dolostone, limestone and thin pelite layers), whereas dense shear planes and anastomosed fractures run a few meters (2–5) within the metarhyolite at the contact with the carbonate. Triassic dolostone and limestone far from the fault zones are characterized by low to moderate fracturing associated with the NW–SE-striking Alpine folding. The fault zone is instead characterized by a core made of a gouge of pulverized carbonatic material (including < 30% of 2–50 mm dolostone and limestone clasts). The gouge of the core zone is bounded by thin (up to 30 cm width) cataclasitic walls of fine-grained rocks fairly homogeneous in size. In the surrounding damage zone the fine-grained material envelops randomly distributed clasts heterogeneous in size (from mm- to m-width). These breccia bodies mostly consist of highly angular fragments often shaping "jigsaw" texture (Fig. 6C, G).

In the breccia domains, the larger clasts are angular, broken and contain several fractures with radial orientation (Fig. 6E). The fracture meshes in and outside the clasts are dilational and filled with whitish/yellowish calcite cement variably mixed with a comminute reddish matrix (Fig. 6B–E, G). The amount of cement may volumetrically exceed that of the fragments, particularly close to the main slip surfaces, locally accumulating in dilational patches (Fig. 6C, G). Arrays of mm- to cm-thick veins are also common. Brecciated rocks are frequently reopened by cm- to m-thick arrays of fractures filled by large aggregates of euhedral calcite crystals (Fig. 6B).

All the damage zone is pervaded by a multitude of polished slip surfaces with exposed areas from a few cm^2 up to > 100 m^2 (Fig. 7). Polished slip surfaces show multiple sets of striations and slickenlines (Fig. 7). The fibers and slickensides formed by the accretion of fibrous overgrowth. Slickenfibers indicating downdip, oblique or nearly pure strike-slip motions. Oblique to strike-slip kinematic dominates over the large part of the polished slip surfaces and commonly overprint the down-dip striation (Fig. 7). Locally, a progressive curvature of the slickensides from downdip to oblique slip is observable (Fig. 7C, D). Nevertheless, in some cases, polished surfaces with oblique slickenfibers are overprinted by new calcite cement overgrowths, in turn sheared by downdip slip surfaces (Fig. 7C-D).

4.2.2 Outcrop 2 (monte dei marmi)

The second studied outcrop of the *Horse Head Fault zone* is located near Boissano village, close to the summit of Monte dei Marmi (Fig. 2C). Here the fault zone couples Triassic quartzite with Triassic dolostone and limestone and Jurassic marble (Figs. 2C, 3, 5B). Quartzite and dolostone bodies involved within the fault zone are up to ~ 80 m-tick, whereas the deformed domain of Jurassic marble is only ~ 5 m-tick. This latter is constituted by a cataclasite with clasts of mm- to cm- size (Fig. 8A). Coarser clasts are often organized in layers enveloped by finer matrix. Outside this relatively thin deformation zone, marble displays only m-spaced fractures and arrays of veins. Differently, the quartzite fault zone is characterized by a number of thin cores hosted by the larger damage zone (Fig. 8B). Fault cores consist of cm- to dm-thick phyllosilicate-rich shear planes, rarely associated with polished slip surfaces (Fig. 8B, C).

Shear planes are mostly constituted by comminuted gouge, including a fraction of angular clasts heterogeneous (mm- to dm) in size (Fig. 8C–E). Brecciated texture characterizes instead the quartzite apparently lacking phyllosilicate content. Cohesive, chaotic quartzite breccia constitutes the wide damage zone branching small lenses of less deformed rocks where the polyphase metamorphic schistosities are preserved (Fig. 8D). Alternation of dolostone and limestone crosscut by the fault zone show the same characteristics of the Verzi outcrop, as they are characterized by well-developed cohesive chaotic breccia crosscut by a number of polished slip surfaces. Also the kinematics of the

(See figure on next page.)

Fig. 6 Main features of the *Horse Head Fault zone* exposed in the Verzi abandoned quarry. **A** Damage zone is constituted by alternation of brecciated dolostone, limestone and thin sheared pelite layers, including multiple polished slip surfaces (white arrow highlights one surface of tens of square meters). **B** Brecciated domain with dilational jogs filled by euhedral calcite crystals. **C** The grain size of the crush breccia and cataclasite decreases toward the fault core at the main slip surface (from left to right). **D** Cataclasite supported by a pinkish very fine-grained matrix. **E** Fault breccia with large and broken angular clasts containing fractures with radial orientation, pointed at by red arrows. **F** Heterogranular crush breccia of dolostone in the outer part of the damage zone. **G** Breccia bodies of highly angular fragments with "jigsaw" texture

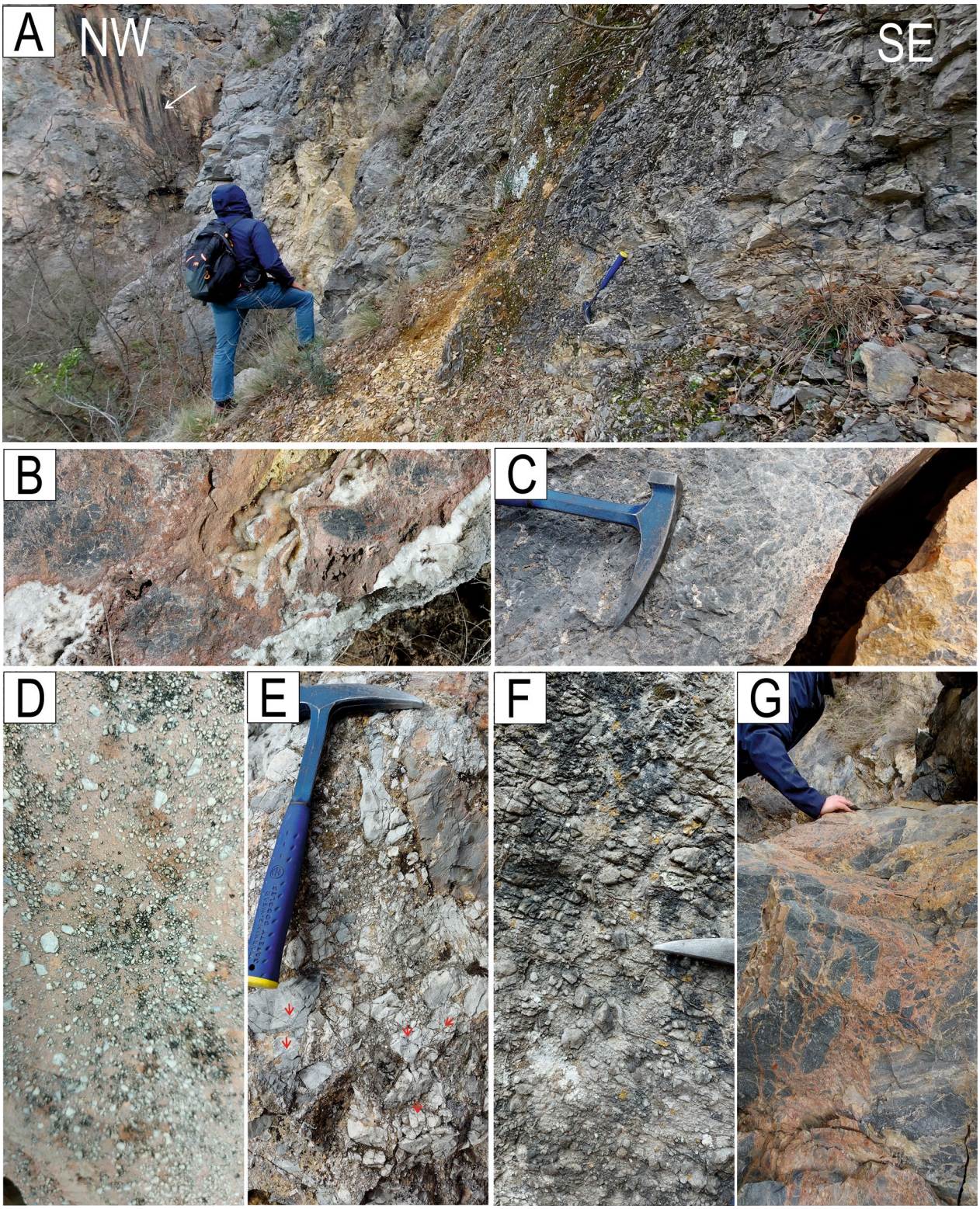

Fig. 6 (See legend on previous page.)

Verzi outcrop is confirmed: dominant oblique-to strike-slip slickenfibers generally overprint downdip striation, but are locally overprinted by relatively younger downdip slickenlines.

4.3 Fault slip data from the field survey

4.3.1 Outcrop 1 (verzi quarry)

Thirty-seven measurements of rake and sense of the fault slip vectors have been collected on exposed slip surfaces in the abandoned quarry close to Verzi village (Fig. 5A). The stereonet summarizing the strike and dip of the fault planes and the trend and plunge of the slickenlines is shown in Fig. 9. The faults measured the field survey in Verzi are labelled FFV (Field Faults Verzi). In the following, the strike of all the faults is always measured as a clockwise angle from the north.

In most cases, the slickenlines suggest that the faults experienced dominant strike-slip motion, although normal slip also occurred more seldom. Field measurements allow to distinguish two main fault groups with opposite kinematics, left- and right-lateral, respectively. The first group of faults (FFV1) has a main strike of 220°, and dip of 84° (Fig. 9A). The slickenlines trend has a main value of 40°, with plunge of 13°. These nearly vertical fault planes have thus strike-slip right-lateral movement, with a negligible normal component. In Fig. 9B is shown a set of other four measurements of faults (FFV2) with similar attitude of planes and slickenlines. The main value of the strike of these faults is 230°, with a dip of 47.5°. The main trend of the slickenlines is 37° and the plunge is 13°. Both the orientation of the planes and the striation are very close to the ones shown in Fig. 9A, although less steep. The orientation of the striation suggests that the slip has a similar normal and right-lateral components.

A third set of faults with similar dip direction and striation trend (FFV3) is shown in Fig. 9C. The main strike of this set of faults is 285°. The dip of these faults is 75°. The main trend of the slickenlines observed on the fault mirrors is 98°, with a plunge of 25°. The field study on these surfaces suggest that the motion was left-lateral. This first family of faults is transpressional with a dominant sinistral strike-slip component and a minor reverse component.

Another recognizable pattern of four fault orientations (FFV4) is shown in Fig. 9D. Fault surfaces have a main strike of 147° and a dip of 40°. The main slickenlines trend is 302°, while the plunge of the lineations is 23°. The analysis of these fault surfaces suggest that they are normal faults, with a comparable component of right-lateral strike-slip.

Figure 9E shows the orientation of all the thirty-seven FFV measurements in one stereonet. The orientations of all measured fault planes and slickenlines are reported. In white and grey, the compressional and extensional domains, respectively. The directions of the strain axes are consistent with the hypothesis that the shear zone is in the strike-slip regime. The first principal strain axis is directed NNW-SSE, while the third one is oriented WSW-ENE. The intermediate strain axis is almost vertical.

The bedding in the area of Verzi has been determined through ten measurements, with a mean dip direction value of 170° and dip of 12° (Fig. 9F).

4.3.2 Outcrop 2 (monte dei marmi)

The field data collected in the area of Monte dei Marmi (Figs. 5B, 10) consist of seventy-five measurements of dip and dip direction of fractures (we called these measurements FFM as in "Field Fractures Monte dei Marmi"). Through the use of the software Stereonet 11, it has been possible to individuate five sets of fracture planes that had similar attitude.

The first set, consisting in sixteen fracture planes (FFM1), is characterized by a main strike of 212° and a dip of 58° (Fig. 10B). The set FFM2 (thirteen measurements) is strictly related to FFM1, since it has a main value of the strike of 218°, but the fractures dip on average at a higher angle, with a dip of 78° (Fig. 10C). Since their orientation is very similar, they are both colored with similar hues of green in Fig. 10A–C.

The third set of fractures (FFM3, consisting in thirteen measurements), has a main strike of 293° and a dip of 69° (Fig. 10D). The fourth set (FFM4, four measurements), has a main value of the strike of 44° and dip of 53° (Fig. 10E). The last recognizable pattern of fractures measured in Monte dei Marmi (FFM5, thirteen measurements) has main strike of 132° and dip of 73° (Fig. 10F).

From the inspection of Figs. 9 and 10, it is possible to find a good agreement between the field measurements collected in Verzi and those collected in the area

(See figure on next page.)

Fig. 7 Representative kinematic features from polished slip surfaces of the Horse Head Fault zone. All pictures are taken from dolostone and limestone outcrops. **A** Oblique slickenlines are exposed on two conjugate fault walls. **B** Dominant oblique slickenlines are overlapped by the down-dip slickenlines, as highlighted in the inset **E**. **C** Polished slip surface showing progressive curvature of the slickenside from down-dip to oblique right-lateral motion. **D** Down-dip normal slickenside on cataclasite (1A) are overlapped by oblique right-lateral striations (1B). **F** Gentle curvature of the slickenline showing right-lateral motion

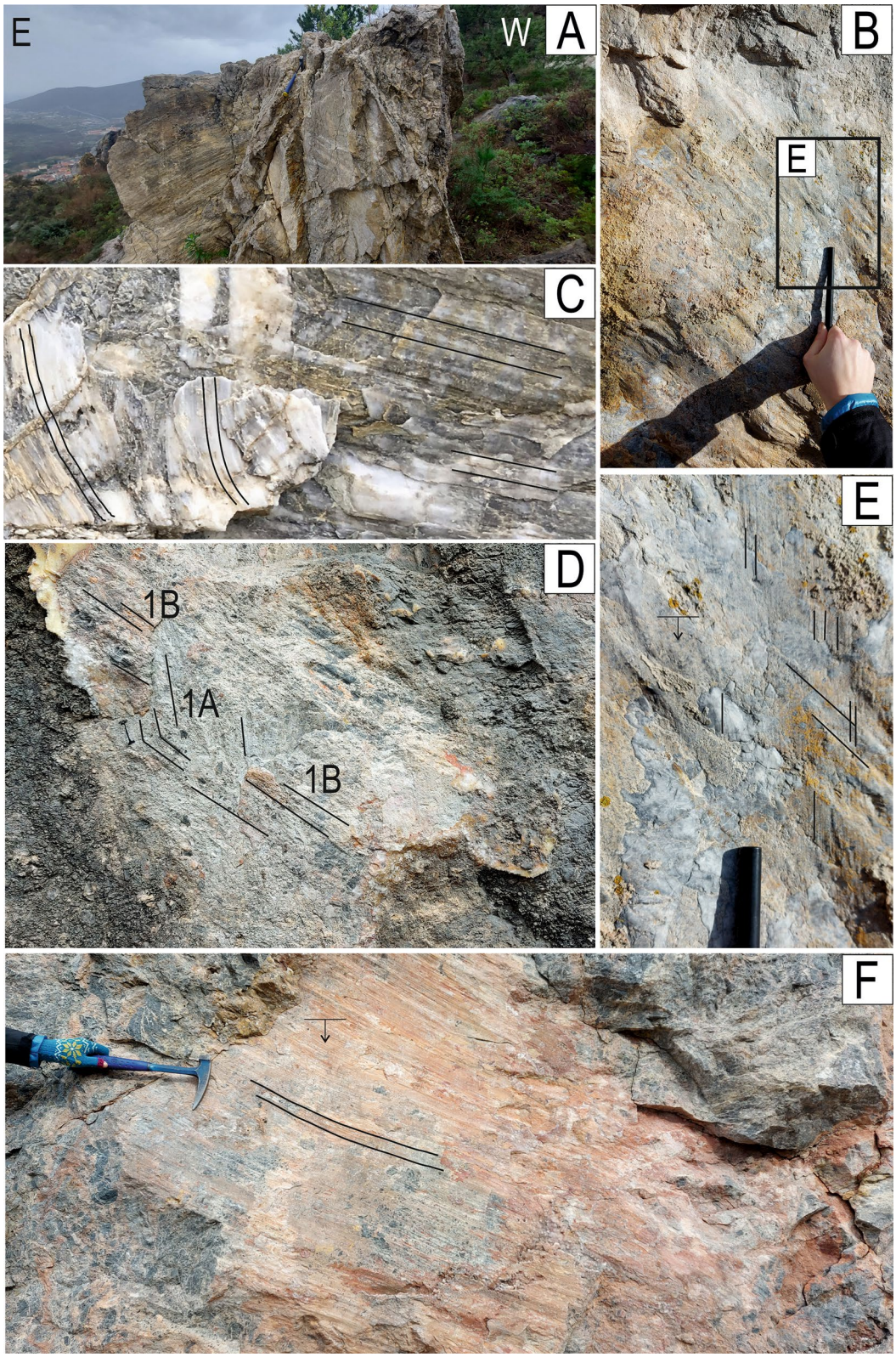

Fig. 7 (See legend on previous page.)

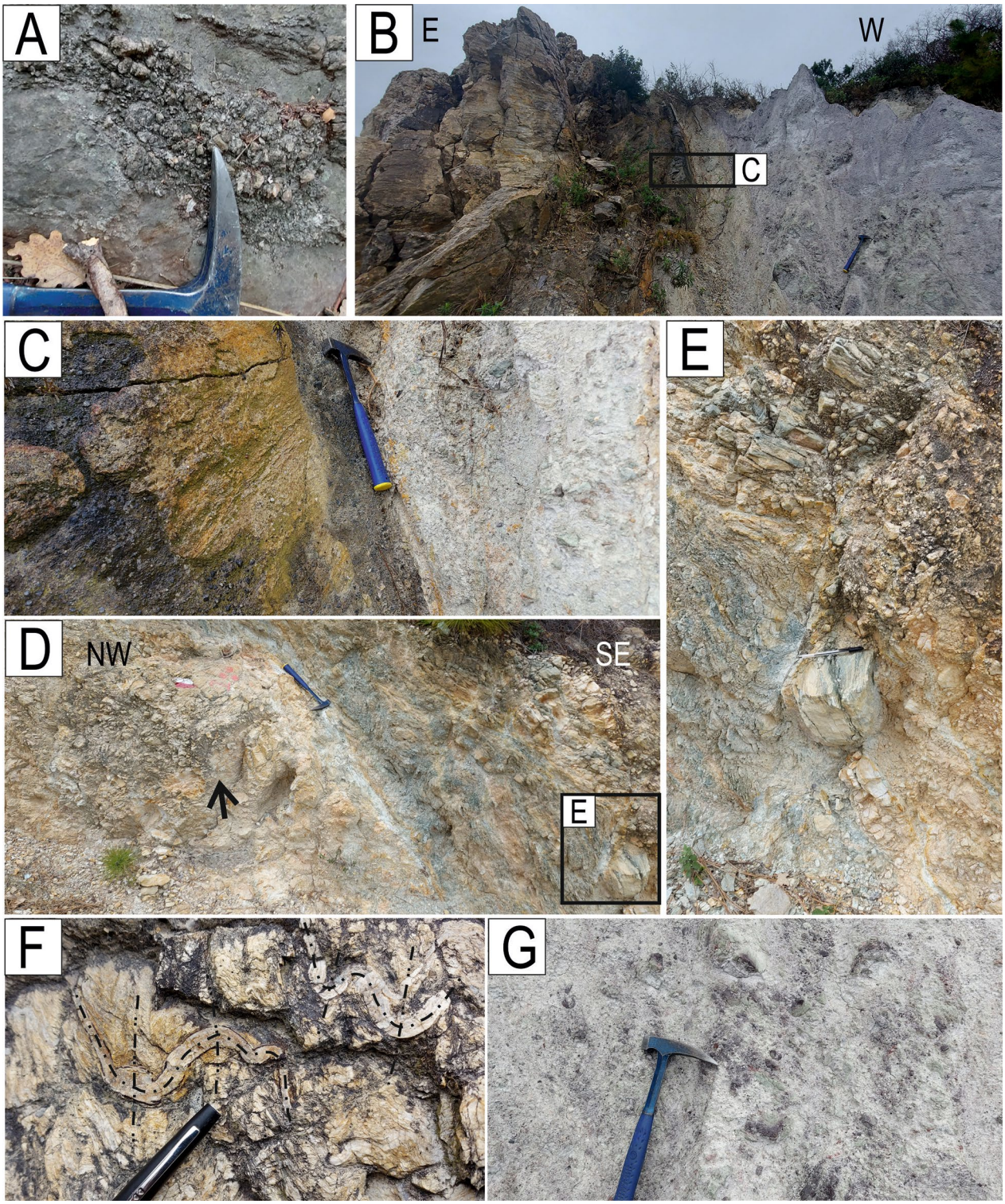

Fig. 8 Main features of the *Horse Head Fault zone* exposed at Monte dei Marmi (Fig. 2). **A** Cataclastic fault core in Jurassic marble. The domain enveloping the large angular clasts is constituted by fine-grained cataclasite. **B** Fault zone at the contact between dolostone-limestone (on the left) and quartzite (on the right). Carbonate rocks form mostly cataclasite of various grain size with slickensides whereas in quarzite fault gouge are dominant. **C** Detail of the contact in **B** showing the comminuted gouge in the fault core. **D** Quartz-dominated domain appears as cohesive breccia of angular clasts (black arrow) and cataclasite, whereas the phyllosilicate-rich layers form shear zones, with relicts (**E**, **F**) preserving the ductile Alpine D1-2 schistosities. **G** Another detail of quartzite gouge contacting large angular clasts

of Monte dei Marmi. In fact, the sets FFM1 and FFM2 from the field survey in Monte dei Marmi have almost the same orientation of sets FFV1 and FFV2 collected in Verzi. Moreover, the set FFM3 has almost the same orientation as the set FFV3.

The average dip direction and dip of the bedding in the area of Monte dei Marmi, calculated from twelve measurements collected during the field survey, are 150° and 50°.

4.4 Fault slip data DOM (verzi quarry)

The fifty-five measurements of fault plane orientation with slickenlines and slip directions are shown in Fig. 11. This set of measures comes from the analysis of the 3D digital outcrop model (DOM) of the Verzi quarry (Fig. 4) outcrop made through the plane and lineation tools of the Compass function on the Cloud Compare software. The preferential strikes of the fault planes are WNW-ESE and WSW-ENE. In most cases, the striae on the fault planes suggest that they are strike-slip faults. The label of these faults is DF (DOM Faults).

The Digital Outcrop Model allowed the measurement of the orientation of fault slip surfaces that were not accessible during the field survey. Therefore, the results from the digital analysis bring to light different strikes of fault and slip orientations. In other cases, the DOM and the field measurements are similar and the main fault planes can be detected.

The most populated group consists of twenty faults with similar orientation, labelled DF1, and shown in Fig. 11A. The main strike of these faults is 307°, and the dip is 80°. The main trend of the slickenlines is 126° and the plunge is 25°. The dominant component of the slip for this set of fault surfaces is strike-slip, with a negligible reverse component. The kinematic indicators suggest that the slip was left-lateral.

The second main set of faults with similar plane and striation orientations, DF2, is shown in Fig. 11B. This data set consists of fourteen measures. The strike of these faults has a main value of 100°, while the dip is 82°. The slickenlines have a main trend of 103°, and the value of the plunge is 23°. These are almost vertical strike-slip faults, with a negligible reverse component. The sense of slip is left-lateral.

A third set of fault and slip directions is shown in Fig. 11C, with a total of six measurements with similar values (DF3). The main value of the strike of this set is 245°, and the dip is 78°. The main striation trend is 62°, with a plunge of 14°. The slip that these faults experienced is mainly strike-slip, but a modest normal component of slip can be observed. The analysis of these surfaces on the digital model suggests that the sense of slip is right-lateral.

Another set of five plane direction measurements with the orientation of the slickenlines is shown in Fig. 11D, and is labelled as DF4. The main strike of the faults is 291°. The dip is 61°. The main trend of the lineation is 103°, while the plunge is 11°. In this case, the faults were characterized by a transpressional regime, having comparable strike-slip and reverse slip components, with left-lateral sense of slip. If we compare the orientation of the planes and the sense of slip of these faults with those of Fig. 11A, we can notice that the two sets share the same surface direction. This set of reverse-left-lateral faults are less vertical than the previous ones. The field analysis of these fault planes suggest that the two sets represent two different phases of deformation that happened consequently, with a first phase of reverse faulting followed by a rotation of the fault plane and a switch to the dominant strike-slip mechanism.

The last recognizable set of faults, DF5, consisting only in two measurements, is shown in Fig. 11E. These faults have a main strike of 263°, with a dip of 42°. The main trend of the lineation is 304°, and the plunge is 11°. These reverse faults have only a negligible strike-slip component. The sense of the slip is right-lateral.

In Fig. 11F, all the fifty-five DOM measurements are plotted in the same stereonet (equal-angle, lower-hemisphere projection). First, all the orientations of the plane and the slickenlines are reported. Furthermore, the white and grey areas represent the fault plane solution of this set of measurements (in white, the compressional domain, in grey the extensional domain), and the colored squares the orientations of the principal strain

(See figure on next page.)

Fig. 9 Stereonets (equal-angle, lower-hemisphere projection) showing the faults mapped during the field survey in Verzi (FFV). The arrows indicate the trend and plunge of the slickenlines. **A**–**D** Stereonets showing the strike, dip, striae trend and plunge of the four main sets of measurements (FFV1, FFV2, FFV3, FFV4) and the standard deviations. The sense of slip can be normal (*N*), reverse (*R*), right-lateral (*RL*) or left-lateral (*LL*). Most sets represent NE-SW right-lateral faults and NW–SE left-lateral faults. **E** Stereonet showing P- and T- axes of all the measured faults. The white and grey areas represent the shortening and the extensional domains, respectively. The blue square represent the direction of the first principal strain axis (1, maximum shortening), the red square the third principal strain axis (3) and the yellow square the direction of the intermediate strain axis (2). **F** Stereonet showing the bedding in Verzi, with the mean value of its dip direction and dip

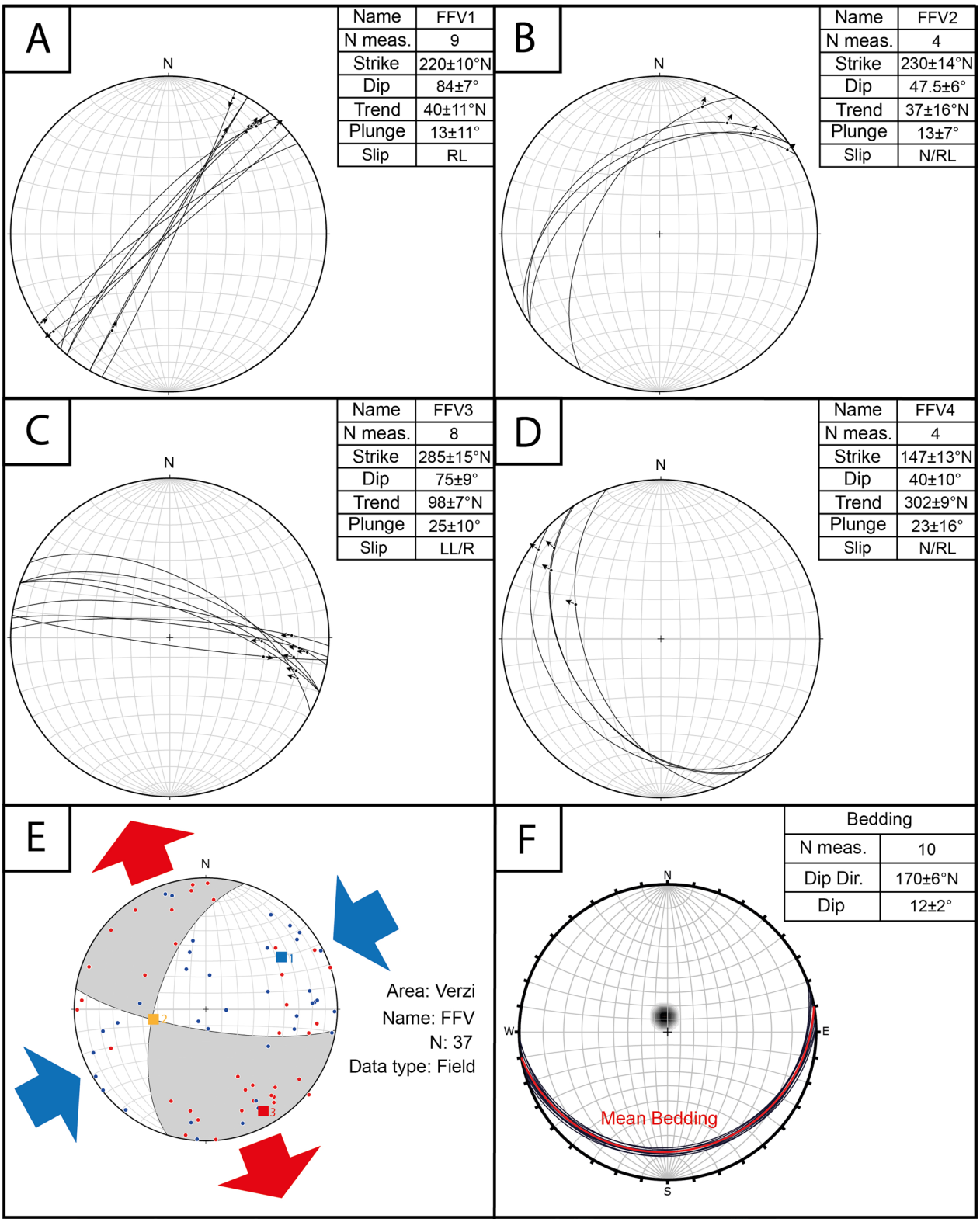

Fig. 9 (See legend on previous page.)

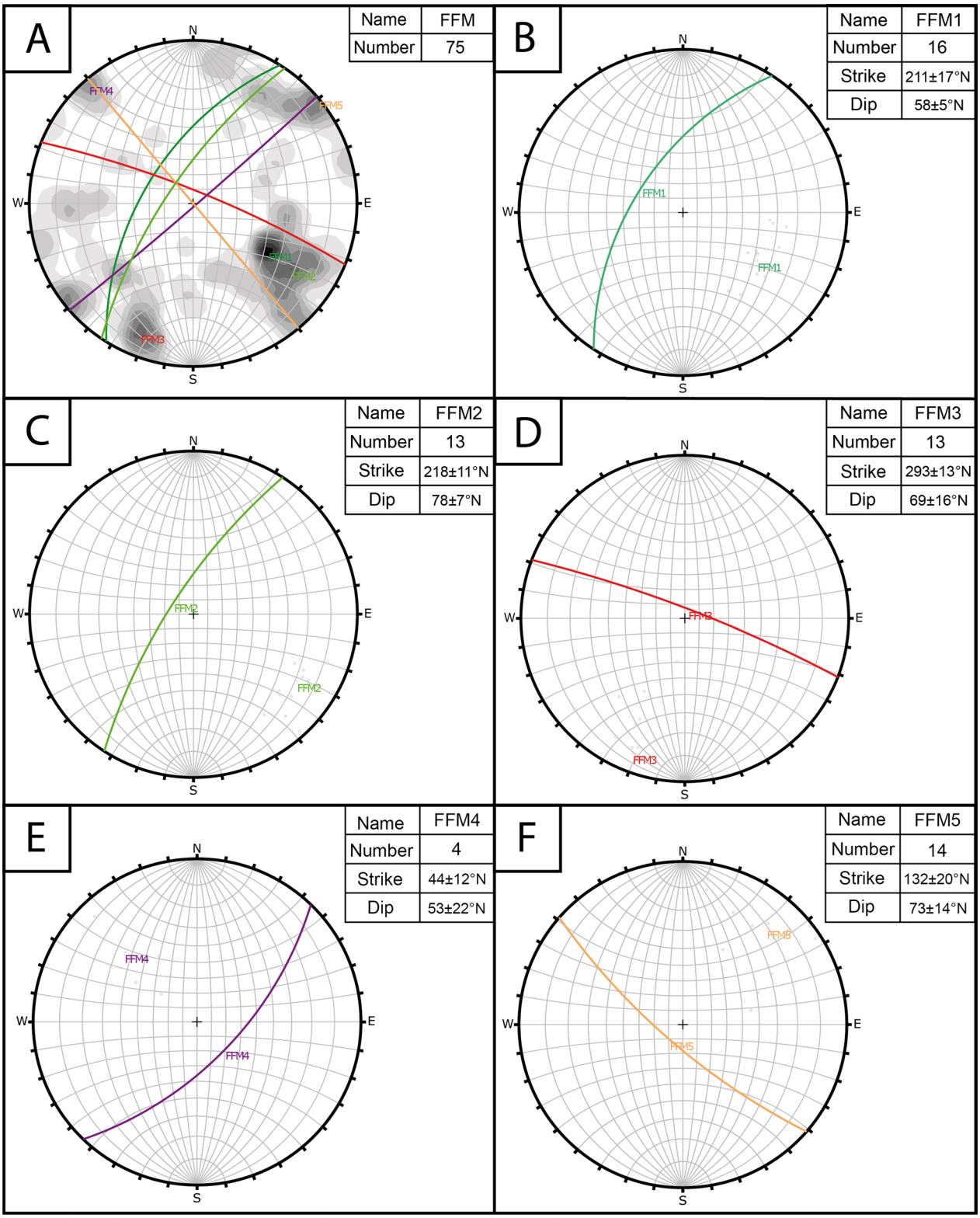

Fig. 10 **A** Stereonet (equal-angle, lower-hemisphere projection) showing the poles of all the fracture planes mapped in the area of Monte dei Marmi, on the Ligurian Alps, through the field survey (FFM). The contouring enlightens the concentration of plane poles. The main sets of fracture planes are also shown. **B**–**F** Main isolated fracture sets (FFM1, FFM2, FFM3, FFM4, FFM5), with plane direction and pole. The strike and dip with the standard deviation are detailed. Stereonet data are lower hemisphere, equal angle projections

axes. The first principal strain axis is directed NNW-SSE, while the third one is oriented WSW-ENE. The intermediate strain axis is almost vertically dipping. The plot suggests that the system is in the transtensional regime.

4.5 Fault slip data verzi, field and DOM

We can now unify the data collected during the field survey (Fig. 9) and those derived from the UAV photogrammetry (Fig. 11). The total number of the measurements is ninety-two (Fig. 12), thirty-seven of which from the field survey (FFV measurements) and fifty-five from the Digital Outcrop Model (DF). The resulting stereonet plot (Fig. 12A) shows an ESE-WNW left-lateral set and a SSW-NNE right lateral set.

Figure 12A shows the orientations of all fault planes measured in Verzi, with arrows that indicate the slickenlines orientation and the sense of slip. Through the use of the Faultkin 8 software, the directions of the major, intermediate and minor strain axes (1,2,3) have been calculated (Fig. 12B). The linked Bingham statistics also allowed to determine the shortening and extensional domains. By a comparison of Fig. 12B, Figs. 9E, 11F, the direction of the principal strain axes calculated from the field data is very similar to that determined from the DOM.

As we can see in Fig. 12B, the shear zone is in the transtensional regime with right-lateral kinematic. The major kinematic component is strike-slip, with a minor normal component. The first principal strain axis, or equivalently the P-axis, is oriented approximately ENE-WSW, while the T-axis is oriented NNW-SSE.

5 Discussion

5.1 The advantages and limitations of digital outcrop model in fault analysis

As already mentioned in previous work (Menegoni et al., 2019; Inama et al., 2020; Panara et al., 2022b), the main advantage of the DOM technique respect to the field-base survey is the possibility to digitally measure at any time and in any place fault and fracture geometry (orientation, size and position) from all the accessible or inaccessible outcrop areas with a safer, quicker and more accurate technique. In addition, this study shows as DOM can be very useful for the fault kinematic analysis: comparing the field and DOM measures of the Verzi quarry, it is clear that DOM allows to measure around 50% faults orientation and kinematics (Figs. 9, 11) and to detect fault sets that can be crucial for the development of a structural model. Nevertheless, DOMs have also limitations, such as the censoring of all the information that are below the DOM resolution and the impossibility to obtain direct-contact information as fault rock composition and texture (Figs. 6–8). Even if recent improvements, as the hyperspectral DOMs (Thiele et al., 2022), can help to overcome the rock composition limit, we think that in geological studies DOMs can improve the structural analysis but cannot replace the traditional field survey.

5.2 Lithology-dependent internal structure of the *horse head fault zone*

Thicknesses up to 250 m of the major fault segments can be correlated with displacements in the order of several hundred of meters to kilometers (Faulkner et al., 2011; Savage and Brodsky, 2011). The entire fault zone therefore accommodated a significant total displacement of several (at least 5–10) kilometers. The different lithologies involved in the faulting processes display a variety of deformation textures. Limestone and dolostone characterized by the presence of angular fragments with jigsaw texture and calcite-filled dilational patches and vein arrays (Figs. 6B and G) support the interpretation that the brecciated rock consist of dilation chaotic breccia (Woodcock et al., 2007; Woodcock and Mort, 2008), associated with a net volume increase during formation (Tarasewicz et al., 2005). The main slip domains show a single, large (up to 3 m) gouge locally surrounded by the huge cataclasites and brecciated damage zone. Differently, the quartzite involved in the fault zone alternate m-sized brecciated bodies (chaotic breccia; Woodcock and Mort, 2008) with phyllosilicate-rich gouges. A further different texture, characterized by cohesive fine grained cataclasite and absence of gouge, is preserved by the marble at the contact with the quartzite, consisting of thin proto-cataclasite. Such differentiated behaviors

(See figure on next page.)

Fig. 11 Stereonets (equal-angle, lower-hemisphere projection) showing the DOM fault slip data (DF) from Verzi. Arrows indicate the trend and plunge of the striae. **A**–**E** Stereonets showing the main sets of faults (DF1, DF2, DF3, DF4, DF5), with strike, dip, striae trend and plunge and the standard deviations. Slip can be normal (*N*), reverse (*R*), right-lateral (*RL*) or left-lateral (*LL*). Most sets represent F left-lateral faults, one set represents NE-SW right-lateral faults and one consists in E-W normal faults. **F** Stereonet showing the P- and T- axes of all the measured faults. Grey and white areas represent the extensional and the compressional domains, respectively. The blue square represents the direction of the first principal strain axis (1, maximum shortening), the red square the third principal strain axis (3) and the yellow square the direction of the intermediate strain axis (2)

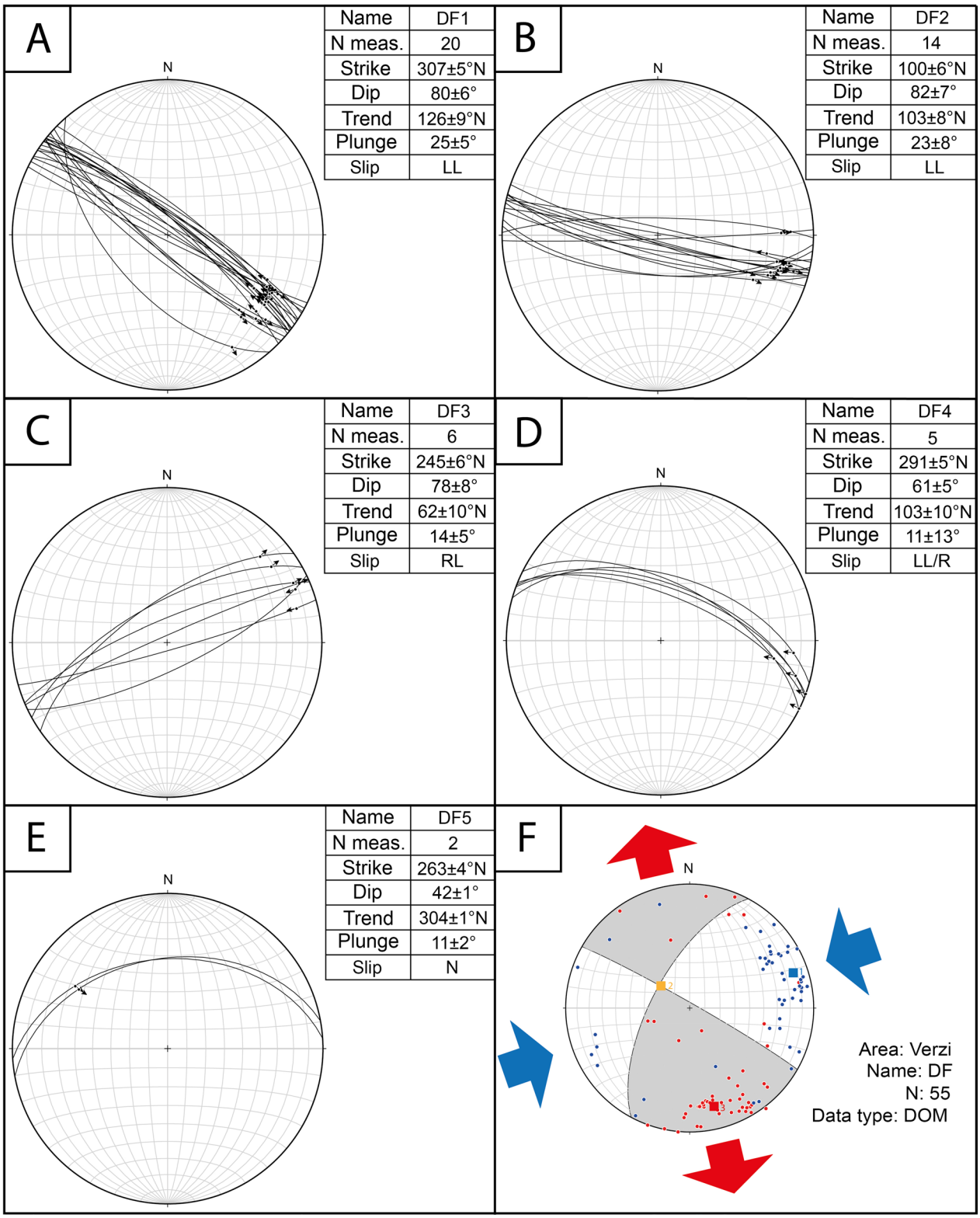

Fig. 11 (See legend on previous page.)

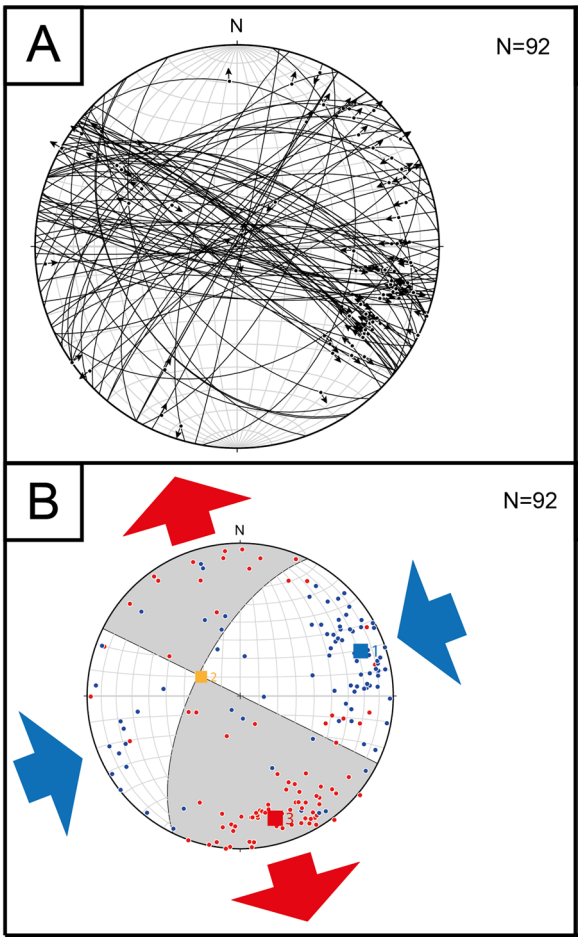

Fig. 12 **A** Stereonet (equal-angle, lower-hemisphere projection) of all ninety-two measurements collected in Verzi, both through the field survey and through the DOM (FFV and DF, respectively). **B** Kinematic axes, fault plane solution and P- and T- axes of all the measured faults. The first principal strain axis (1, labelled in blue color) trends WSW-ENE, the third (3, labelled in red color) trends NNW-SSE. Blue arrows indicate the direction of compression, red arrows the direction of extension

support a falloff of damage as a function of distance from the fault as dependent on the local lithology, aside the displacement. In particular, phyllosilicate-rich assemblages favor shear plane localization (Collettini et al., 2019), as well as heterogeneous composition (alternation of dolostone, limestone and pelite) correlates with wider damage zones with respect to more homogeneous rocks (i.e. marble).

5.3 A Riedel model for the *horse head fault zone*

Map trace of the NE-SW-striking *Horse Head Fault Zone* displays horsetail geometry resembling dextral transtensional structures. In the following, we attempt to link the orientations of the most recognizable sets of faults to the model of the Riedel shears. The Riedel model predicts the formation of subsidiary fractures with different orientations around a main fault (e.g. Berthè et al., 1979; Deng and Zhang, 1984; Davis, 2000; Taylor et al., 2003; Katz et al., 2004; Li et al., 2016). R fractures form a small angle with the main fault Y, typically 15°, and they have the same sense of slip. P fractures are almost symmetrical to R fractures with respect to the direction of the main fault and they also have the same strike-slip sense. Two sets of antithetic fractures are R' and X fractures. R' fractures, in particular, have the opposite sense of slip than that of the main fault and they typically form at an angle of about 75° with Y. X fractures have the same properties than R' but they dip almost symmetrically to R' fractures with respect to the direction of the main fault, only with a slightly smaller angle with Y.

Figure 13 summarizes the orientations of the main planes measured through both traditional field survey and UAV digital photogrammetry.

The fault zone is bounded by ~ 45°N striking fault walls with dextral kinematics. The sets FFV1 and FFV2 measured during the field survey of outcrop 1 (Verzi quarry) have a main strike between 220 and 230° (Fig. 13A) and right-lateral direction of slip. Considering set FFV1 and its standard deviation (about 10°), the orientation of the set forms an angle between 0 and 15° with the average orientation of the main fault. In this range, P fractures predicted by the Riedel model form. However, the overlapping confidence intervals make impossible to distinguish if consider FFV1 as either parallel to the main fault or as P fractures. The set FFV2 has a main strike very similar to that of the main fault. It may be interpreted as a part of the main fault or as the product of a precedent phase of deformation of FFV1. In fact, the analysis of orientation, dip, and slip direction of the sets FFV1 and FFV2 suggest that these sets may likely be products of two subsequent stages of deformation on the same fault plane. One exposed fault wall shows an orientation that lays between those of these two sets and two sets of lineation can be detected on it. One set of slickenlines indicates clearly down-dip shearing, while the second is an indicator of right-lateral strike-slip motion (Figs. 7D, E).

The set of faults FFV3, with a main value of the strike around 285° and a standard deviation of 15°, consists of left-lateral faults (Fig. 13A). In this case, the angle between the set and the main fault is between 45° and 75°. Since the sense of the slip is opposite to that of the main fault (Fig. 13A) and given the large angle measured between the main fault and these sets of secondary faults (around 60°), these faults can be interpreted as antithetic R' fractures in the framework of the Riedel model. Moreover, if the orientation of set FFV1 was interpreted as the local orientation of the main fault in Verzi area, the angle

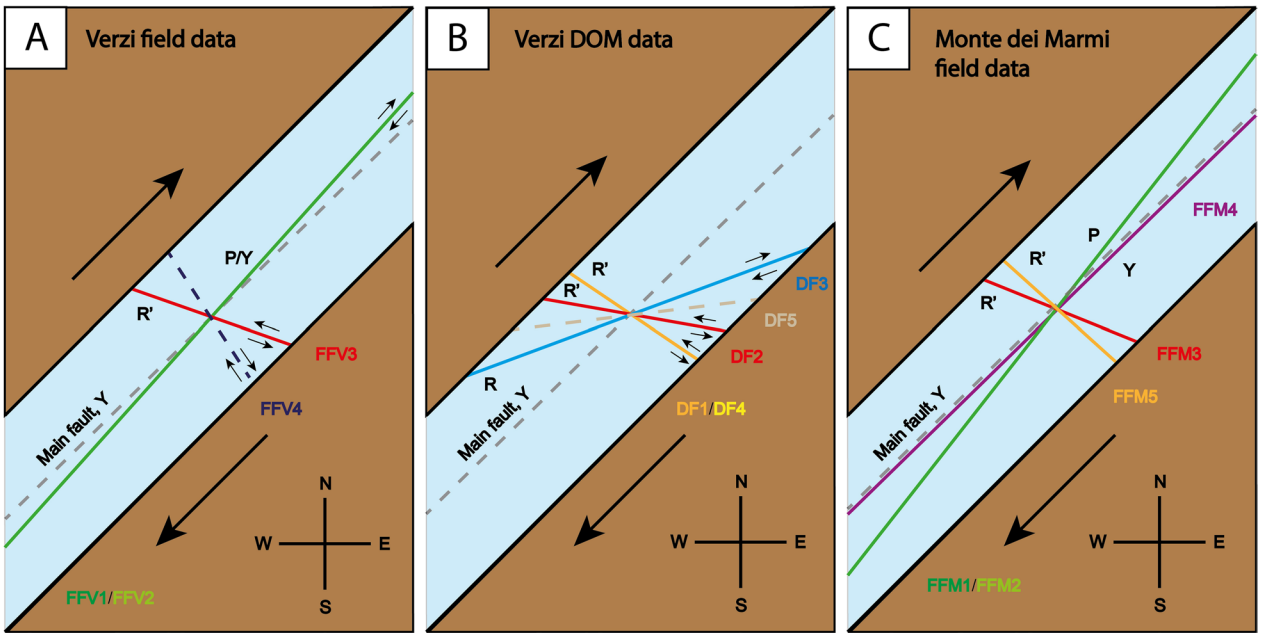

Fig. 13 Interpretation of the measured fault slip data in the frame of a Riedel model (e.g., Berthè et al., 1979). See text for explanation. **A** FFVs are the main sets of faults measured in the Field from Verzi. **B** DFs are the main trends of faults from the Digital Outcrop Model of Verzi. **C** FFMs are the main sets of fractures measured in Monte dei Marmi

between this set and FFV3 may lay around the value of 70° or higher, which is more consistent with the angle of the R' shear fractures.

An additional reason to consider the set FFV1 as representative of the local orientation of the main fault is that the data obtained through the field survey were taken in an area in Verzi (Fig. 2B), which was closer to the core of the main fault than those obtained through the digital model (Figs. 2B, 3). This may be the reason why the orientation of the main trends of faults differ between the two datasets. It may also explain why some of the measurements form the field survey appear to be parallel or sub-parallel to the average strike of the main fault.

Considering the measurements collected by DOM, the set DF1 of left lateral faults has a main strike of 307° (Fig. 13B). Also in this case, the large angle with the strike of the main fault (around 80°), and the opposite sense of slip suggest that these faults may also be interpreted as antithetic R' fractures in the Riedel shear model. The set DF1 appears to be related to the set DF4, also consisting in left-lateral faults with a thrust component. The set DF4, in fact, has a similar main strike (291°). As in the case of the sets of faults FFV1 and FFV2, the sets DF1 and DF4 may represent two different phases of slip along the same fault plane. The fact that the same slip surface witnesses the presence of both downdip and strike-slip slickenlines indicates that faulting accomplished in two distinct stages. A fault that was initially reverse may have experienced a rotation that led to strike-slip movement.

The set DF2, striking at 100°, forms an angle of around 55° with the orientation of the main fault (Fig. 13B). It has a sinistral kinematic that suggests that it may correspond to a R' fracture, although the angle with the main fault is lower than that typical of R' Riedel fractures, even considering the standard deviation, of about 6°. The set DF2 is very close, both in orientation and sense of slip, to the field set FFV3 (Fig. 13A), which, as already discussed, may be interpreted as a R' fracture in case the local direction of the main fault is 220° as the sets FFV1 and FFV2. In this case, the angle between DF2 and the main fault could reach a value of about 65°, closer to the typical angle between the mean fault and the antithetic R' fractures.

Finally, the set of right lateral faults DF3, with a main strike of 245° forms an angle of about 15° with the main fault (Fig. 13B). In the hypothesis that the angle of internal friction ϕ of this rock is around the typical value of 30°, the angle between the main fault and the secondary faults corresponds to half the value of ϕ. This suggests that this set of faults are very likely the synthetic R fractures of the Riedel framework.

Considering now the measurements collected during the field survey in the area of Monte dei Marmi, near the small town of Boissano, the interpretation of the fracture orientations is presented in Fig. 13C. Sets FFM1 and

FFM2, with main strike of 212° and 218° respectively, have both a very similar trend to that of the field set of faults FFV1 (main strike of 220°) (Fig. 13A and C). They form an angle of about 10° with the average direction of the main dextral strike slip faults, which is consistent with the direction of P fractures. Since the standard deviation on this two sets of measurements is quite high (17° for set FFM1, 11° for set FFM2), and given the small difference with the main strike of the main fault, it is also possible that these sets of measurements represent the local orientation of the main fault.

The set FFM3, striking at 293°, may represent a set of antithetic R' fractures, with an angle of 68° to the direction of the main fault (Fig. 13C). This set has a very similar orientation to that of the field set FFV3 and the DOM set DF2, collected in Verzi (mean strike of 285° and 100°, respectively) (Fig. 13A, B). It is worth noting that the set DF2 has a strike which differs from those of FFM3 and FFV3 of more than 180°. This is due to the fact that all three these sets of planes of discontinuities dip at a large angle, so that no significant difference in orientation exists between almost vertical planes striking at angles that differ of 180°.

The set FFM4, striking at 44°, has almost the same average orientation of the main fault (Fig. 13C). This suggests that the set of fractures FFM4 measured in Monte dei Marmi formed under the same stress conditions and in the same direction of the Horse Head fault (45°).

Finally, the set FFM5 strikes at 132°, very close to the strike of the DOM sets DF1 and DF4 (mean strike around 300°), forms an angle of ~ 87° with the orientation of the main fault strike (Fig. 13B, C). Given a standard deviation on this set of measurements of about 20°, this suggests that also FFM5 fractures may be interpreted as R' Riedel fractures.

From the inspection of Fig. 13, it is clear that the field measurements collected in Monte dei Marmi have a surprisingly good agreement with both the field and DOM measurements collected in the area of Verzi. It is likely that the sets of fractures in Monte dei Marmi formed under the same state of stress than that responsible for the formation of the fault system discovered in Verzi.

5.4 Kinematics of the *horse head fault zone*

Overall, the fault slip data and analysis indicate that the fault network encompassed by the Horse Head Fault Zone is compatible with a ~ 15 km-wide Riedel shear zone formed under a dominant dextral strike-slip regime. The horsetail geometry envisaged by the map-view of the fault network thus confirms the presence of a large transtensional structure, running roughly parallel to the present coastline (Fig. 2C). However, the dominant right-lateral kinematic was pre- and post-dated by fairly normal faulting as evidenced by the superimposition of different generations of slickenlines (Fig. 7). In particular, both FFV1, FFV2 and FFV3 sets locally show progressive curvature of the slickenlines from downdip to the dominant oblique motion. On the other hand, slickenlines associated with the strike-slip movement are locally superimposed by new calcite fibers shared by downdip striations (Fig. 7). Therefore, it results that the Horse Head Fault Zone kinematic experienced either multiple changes in the local orientation of the stress fields, a rotation of the structure or a combination of the two. In fact, due to the lacking of absolute ages, it is impossible to discriminate if the different kinematic was associated local flips of stress axes during the same event (e.g. Cardello and Mancktelow, 2015) or, differently, as a marker of discrete deformation phases.

5.5 Timing

The development of the Horse Head Fault Zone clearly postdates the schistosities (Fig. 8E, F) associated with the ductile phases recognized in the Ligurian Alps (D1-3; Vanossi et al., 1984; Seno et al., 2005; Bonini et al., 2010). On the other hand, we cannot exclude that the present-day structure may be the result of the partial reactivation of the inherited compressional architecture (e.g. Tavarnelli et al., 2004; Butler et al., 2006). In fact, the strike of the Horse Head Fault is parallel to the main direction of tectonic transport (from NE to SW) and coincides with the boundary between the different tectonic units. It may be thus speculated that the precursors of the Horse Head Fault Zone were tear faults accommodating the movements of the thrust sheets occurring at different rates of propagation due to differential shortening of the nappe stack (Bonini et al., 2010). Nappe stacking and related folding are dated in the Ligurian Alps in the late Eocene—early Oligocene times. In particular, zircon (U-Th)/He dating of the Penninic Front constrains at ~ 28–32 Ma the thrust propagation in the external Ligurian Alps (Maino et al., 2015a, b). The integration of the depositional ages of the post-collisional sediments (TPB and Finale Ligure Basin; Boni et al., 1968; Gelati et al., 1998; Dallagiovanna et al., 2010) with the thermochronological dataset (Carrapa et al., 2003; Maino et al., 2012; Amadori et al., 2023) confirms that the Ligurian orogen accomplished the exhumation path from depth to the shallow crustal level in the Rupelian (~ 35–32 Ma) although unusual high geothermal gradient (40–50 °C/km), associated with mantle upwelling, affected both the TPB and Ligurian orogen up to the Chattian (~ 28 Ma; Amadori et al., 2023). During the Chattian time, TPB deposits record a switch from extensional to transtensional faulting at few km of depth (Maino et al., 2013; Federico et al., 2014; 2020). Since the Miocene, evidence of deformation are limited to local

transtensive/transpressive faulting and folding of the stratigraphic record (Piana et al., 2006; Federico et al., 2014). The absence of significant strike-slip displacement of the Miocene deposits of the Finale Ligure Basin (Fig. 2C) indicates that the main activity of the Horse Head Fault Zone predates the Miocene. On the other hand, syn-depositional normal faulting is recorded by the Pliocene deposits both onshore and offshore (e.g. Foeken et al., 2003; Larroque et al., 2009; Morelli et al., 2022).

Overall, the integration of geological and thermochronological constraints, suggests that the main strike-slip activity of the Horse Head Fault Zone occurred in the Late Oligocene, coeval with the transtensional faulting in the TPB. Without absolute dating, the evidence of extensional kinematic, both preceding and following the strike slip activity, cannot be confidentially linked to a specific tectonic stage. However, normal faulting predating the HHF strike-slip activity is largely recorded in the late Rupelian—early Chattian TPB deposits, soon after the end of the main Alpine ductile tectono-metamorphic phases (Maino et al., 2012; 2013; 2015a; Amadori et al., 2023).On the other hand, post-Oligocene deformation in the study area are documented in the Early-Middle Miocene shallow deposits of the Finale Ligure basin (Mueller et al., 2023), as produced by multiple seismic inputs coevally with the oceanic spreading of the Liguro-Provençal basin and the Corsica-Sardinia drifting. However, the seismically-related soft-sediment deformation structures are not diagnostics of the related deep fault kinematics. Later in the Pliocene, extensional faulting is instead documented as driving the sedimentation in the Messinian paleo valleys (Boni et al., 1985; Marini 2000; Foeken et al., 2003; Breda et al., 2007; 2009). Further investigations on the relationships between deep faults and shallow shear bands within the Miocene-Pliocene deposits, as well as the offshore record, are needed to fully describe the possible switch between dip-slip and strike-slip faulting in the Ligurian margin since the Miocene.

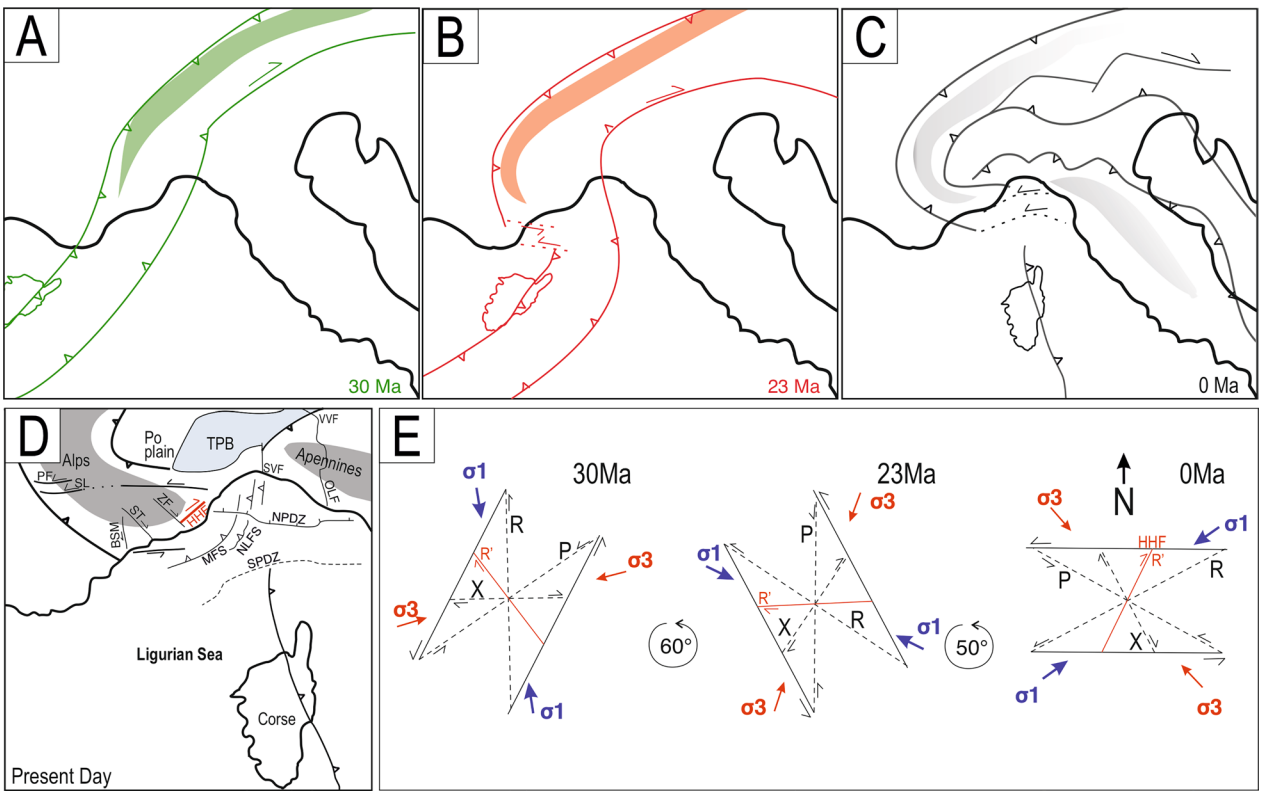

Fig. 14 **A**–**C** Evolutionary sketches of the curvature of the Western Alps; green, red and grey colored lines represent the Alpine fronts at 30 Ma, 23 Ma and present day, respectively. Dotted lines indicate the location of the shear zone of the Ligurian Alps at 23 (red) and present day (grey). **D** Regional tectonic sketch locating the Horse Head fault zone within the mega shear zone (Riedel scheme) represented by the entire Ligurian Alps. The other major fault zones are shown, including *BSM* Breil-Sospel-Monaco fault, *MFS* Marcel Fault System, *NLFS* North Ligurian Fault System, *NPDZ* Northern Principal Deformation Zone, *SL* Stura line, comprising the Stura and Preit faults, *SPDZ* Southern Principal Deformation Zone, *ST* Saorge-Taggia fault, *TPB* Tertiary Piedmont Basin, *ZF* Zuccarello fault. Modified from Maino et al. (2013), Federico et al. (2014), Morelli et al. (2022). **E** Reconstruction of the paleo-orientation of the Ligurian Alps shear zone, restoring the rotation throughout the Chattian and Early Miocene stages

5.6 Tectonic model in the frame of the alpine dynamic

The Horse Head Fault Zone is a ~ 15 km size right-lateral Riedel shear zone inserted in a regional framework displaying several major faults with different strike and kinematics (Figs. 13 and 14). Toward north, the Ligurian Alps are bounded by the WNW-striking Stura and Preit lines (SL in Fig. 14D) that are described as sinistral strike-slip faults, accumulating about 40–50 km of displacement since the Oligocene (Fig. 14; Ricou et al., 1986; Giglia et al., 1996). The internal Western Alps experienced Oligocene to Early Miocene extensional mostly parallel to the axial belt associated with dominant right-lateral displacement along the major faults, such as the Chamonix Line, Pennine Basal Thrust, Briançonnais Front, the Insubric Line and the Simplon-Rhone Fault (Fig. 14; e.g. Sue and Tricart, 2003; Champagnac et al., 2006; Malusà et al., 2009; Molli et al., 2010; Campani et al., 2010; Perrone et al., 2011; Schmid et al., 2017).

To the east, the Ligurian Alps were bounded by the Sestri-Voltaggio Fault Zone, which acted as a transpressive mylonitic shear zone during the metamorphic Alpine phases (D1–D3), and then evolved toward an Oligo-Miocene dextral strike-slip brittle fault system (Capponi et al., 2009; Federico et al., 2009; 2014). East to the Sestri-Voltaggio Fault, the Villalvernia-Varzi Fault and the Ottone-Levanto Fault acted as a sinistral transpressional shear zones during the Late Eocene-Early Oligocene (Fig. 14; Marroni and Treves, 1998; Marroni et al., 2019). The Villalvernia-Varzi evolved as a major left-lateral transpressive fault in the late Oligocene/Early Miocene (e.g. Elter and Pertusati, 1973; Laubscher et al., 1992; Miletto and Polino, 1992). In this framework, the Sestri-Voltaggio and Ottone-Levanto faults represent minor Riedel faults kinematically related to the Villalvernia-Varzi Fault (Fig. 14; Spagnolo et al., 2007; Crispini et al., 2009).

Other important structures in the western Ligurian Alps are two major sub-vertical conjugate strike-slip fault systems: the NE-SW sinistral Breil–Sospel–Monaco (BSM) line and the dextral NW-SW Saorge Taggia (ST) (Gèze and Lanteaume, 1963; Bulard et al., 1975, Decarlis et al., 2014). Offshore, the arcuate (from E-W to N-S trending) compressive fronts of the Marcel Fault System (MFS) and North Ligurian Fault System (NLFS), crosscut the roughly E-W left-lateral Northern and Southern Principal Deformation Zone (NLFS), affecting the Ligurian-Provençal basin (Larroque et al., 2009; Morelli et al., 2022).

The present-day configuration of this fault networks fits with a mega left-lateral shear zone, where the Horse Head Fault Zone represents a R' antithetic fault. Therefore, we argue that the Ligurian segment of the Western Alps accumulated km-scale of main left-lateral displacement during the Late Oligocene times, in agreement with the TPB record (Maino et al., 2013; Federico et al., 2014).

On the basis of this geometry and the estimated rotation of the Ligurian Alps and TPB (~ 117 and ~ 50°, respectively; Collombet et al., 2002; Maffione et al., 2008), the following evolutionary model composed of two consecutive rotational processes is proposed for Ligurian Alps. Soon after the Adria-Europe collision at ~ 35 Ma (Schmid et al., 1996; Ford et al., 2006; Handy et al., 2010; Kästle, 2020; Le Breton et al., 2021), NW dipping subduction zone in west Mediterranean started to roll back while Adria rotated counterclockwise with respect to Europe causing NW- and North- directed shortening at its northern margin. The first manifestation of Liguro-Provençal Basin-related magmatism are dated at 32–30 Ma, coeval with extension in the Ligurian Alps, TPB and Corsica-Sardinia (De Voogd et al., 1991; Serrane, 1999; Brunet et al., 2000; Rossetti et al., 2001; Réhault et al., 2012; Maino et al., 2013). The down-dip striations crosscut by the strike-slip ones on the HHF fault mirrors may represent relics of this early Oligocene extensional regime developed in a such broad area. Since the late Rupelian (~ 30 Ma), strike-slip tectonic in the Ligurian Alps, as well as in the rest of the Western Alps accommodates the relative rotation between the Adriatic and European plates. During this period, the progressing east migration of the Apennine subduction trench caused the opening of the back-arc basins and the Adria and Western Alps counterclockwise rotation (e.g. Carminati et al., 2012). Rotations increased toward the Ligurian Alps that acted as a mega left-lateral shear zone bounding the southern tip of the Western Alps. The dominant strike-slip kinematic recorded by the HHF testify this tectonic phase were displacements of several tens of kilometers were accomplished. We argue that a large part (~ 60–70°) of the ~ 117° counterclockwise rotation recorded by the Ligurian Alps after the metamorphic deformation was accomplished in this time span (from 30 to 23 Ma; Fig. 14).

Since the Aquitanian, left-lateral shearing went out, and the ~ 50° of rotation recorded by the TPB sediments was mainly acquired through passive rotation driven by the Corsica-Sardinia drifting following the West Mediterranean roll back (Faccenna et al., 2004; Maffione et al., 2008). In this period, the seismic deformation recorded in the Early Miocene shallow sediments of the Finale Ligure Basin (Mueller et al., 2023), testifies the activity of the deep faults controlling the rotation. The local evidence of down-dip striations crosscutting the dominant strike-slip ones, could document a kinematic switch from transtension to extension. However, the impossibility to constrain the age of the younger

slickenfibers, does not allow to correlate this structures with tectonic stages.

Finally, as revealed by paleomagnetic data, the Ligurian Alps, and thus the Adriatic plate did not experienced significant rotation since the Late Miocene times and the Pliocene-present day tectonics was controlled by extension followed by recent compressive inversion (e.g. Larroque et al., 2009; Morelli et al., 2022).

6 Conclusions

Thanks to the integration/combination of traditional field-survey and DOM data it has been possible to overcome the main limits of these two technique, and recognize and describe a previously unreported large fault zone.

In this paper we present the discovery and the description of a new large fault zone—named Horse Head Fault zone (HHF)- in the western Ligurian Alps, which provides evidence for a megastrike-slip shear zone involving the southernmost tip of the Western Alpine arc during the late Oligocene.

The HHF is ~ 15 km long and up to 250 m thick and involves several lithologies, including quarzite, metarhyolite, marble and alternation of dolostone-limestone and minor pelite. It is characterized by a complex structure where gouge, cataclasites and brecciated alternate within the damage zone. The fault zone contains a multitude of polished slip surfaces preserving multiple sets of striations and slickenfibers. The dominant kinematic is strike-slip, although evidences of both preceding and following down-dip slip surfaces occur. The HHF is consistent with a km-size dextral NE-SW-striking Riedel shear zone, in turn representing an antithetic R' of the regional sinistral shear zone shaped by the whole Ligurian Alps. Such shear zone accommodated tens of km-scale displacements related to the Adria counterclockwise rotation after the Adria-Europe collision and the start of the rollback of the Apennine subduction. In the Early Miocene, this major fault-system ceased its activity, showing minor extensional (possibly Pliocene) re-activation. Such tectonic framework combined with the existing paleomagnetic data allow to suggest that the large rotation experienced by the Ligurian Alps (117°) developed throughout two consecutive steps. A first late Rupelian-Chattian rotation (~ 60–70°) controlled by left-lateral shear and a second Early Miocene ~ 50°passive rotation driven by the Corsica-Sardinia drifting.

Acknowledgements
We would like to express our gratitude to Maurizio Marino (Ispra) and Simone Fabbi (University of Rome "La Sapienza") for the many fruitful discussion in the field and their constant support to the project.

Author contributions
LM was responsible of both field and Digital Outcrop Model data collection, data analysis and interpretation. MM conceived the work and was responsible of the field data collection and interpretation. MP, NM and ST contributed to the field survey and of the building and interpretation of the Digital Outcrop Model. LC and LF gave a substantial contribution in data interpretation. SS and LC provided the project management and coordination. All authors read and approved the final manuscript.

Funding
This research was supported in the frame of the Italian 1:50.000 Geological Mapping project—CARG Foglio 245—Albenga (ISPRA, Regione Liguria, University of Pavia and Genova).

Availability of data and materials
The datasets collected during the field surveys and analyzed during the current study are available from the corresponding author on reasonable request. The 3D Digital Outcrop Model of the Horse Head Fault zone and of the quarry near Verzi village are freely viewable on the Sketchfab website at the following links: https://skfb.ly/oGrwX. https://skfb.ly/oGtqW and are available from the corresponding author on reasonable request.

Declarations

Ethics approval and consent to participate
Not applicable.

Consent for publication
Not applicable.

Competing interests
The authors declare that they have no known competing financial interests or personal relationships that could have appeared to influence the work reported in this paper.

Author details
[1]Department of Earth and Environmental Sciences, University of Pavia, via Ferrata 1, 27100 Pavia, Italy. [2]Ali I. Al-Naimi Petroleum Engineering Research Center (ANPERC), King Abdullah University of Science and Technology (KAUST), Thuwal, Saudi Arabia. [3]Department of Earth Environment and Life Sciences, University of Genoa, Genoa, Italy. [4]Institute of Geosciences and Earth Resources of Pavia, C.N.R, Pavia, Italy.

Received: 3 May 2023 Accepted: 12 September 2023
Published online: 04 October 2023

References

Agisoft Metashape. Agisoft LCC, St. Petersburg, Russia. Available online: https://www.agisoft.com. Accessed on 1 January 2023.
Allmendinger, R. W., Cardozo, N., & Fisher, D. M. (2011). *Structural geology algorithms: vectors and tensors*. Cambridge: Cambridge University Press.
Amadori, C., Maino, M., Marini, M., Casini, L., Carrapa, B., Jepson, G., & Di Giulio, A. (2023). The role of mantle upwelling on the thermal history of the Tertiary-Piedmont Basin at the Alps-Apennines tectonic boundary. Basin Research, 35(3), 1228-1257.
Angelier, J. (1989). From orientation to magnitudes in paleostress determinations using fault slip data. *Journal of Structural Geology, 11*(1–2), 37–50.
Angelier, J. (1990). Inversion of field data in fault tectonics to obtain the regional stress—III. A new rapid direct inversion method by analytical means. *Geophysical Journal International, 103*(2), 363–376.
Angelier, J., & Mechler, P. (1977). Sur une methode graphique de recherche des contraintes principales egalement utilisables en tectonique et en seismologie: la methode des diedres droits. *Bulletin De La Société Géologique De France, 7*(6), 1309–1318.
Bellian, J. A., Kerans, C., & Jennette, D. C. (2005). Digital outcrop models: applications of terrestrial scanning lidar technology in stratigraphic modeling. *Journal of Sedimentary Research, 75*(2), 166–176.

Berthé, D., Choukroune, P., & Jégouzo, P. (1979). Orthogneiss, mylonite and non coaxial deformation of granites: the example of the South Armorican Shear Zone. *Journal of Structural Geology, 1*(1), 31–42.
Boni, A., Boni, P., Peloso, G. F., & Gervasoni, S. (1985). Nuove osservazioni e considerazioni sui lembi pliocenici dal confine di stato a capo sant'ampelio. *Mem Della Soc Geol Ital, 30*, 246–309.
Boni, P., Mosna, S., & Vanossi, M. (1968). La pietra di finale (liguria occidentale). *Atti Dell'istituto Geologico Dell'università Di Pavia, 18*, 102–150.
Bonini, L., Dallagiovanna, G., & Seno, S. (2010). The role of pre-existing fault in the structural evolution of thrust systems: insights from the Ligurian Alps (Italy). *Tectonophysics, 480*(1–4), 73–87.
Brandano, M., Tomassetti, L., & Virgilio Frezza, V. (2015). Halimeda dominance in the coastal wedge of pietra di finale (Ligurian Alps, Italy): the role of trophic conditions. *Sedimentary Geology, 320*, 30–37.
Breda, A., Mellere, D., & Massari, F. (2007). Facies and processes in a Gilbert-delta-filled incised valley (Pliocene of Ventimiglia, NW Italy). *Sedimentary Geology, 200*(1–2), 31–55.
Breda, A., Mellere, D., Massari, F., & Asioli, A. (2009). Vertically stacked gilbert-type deltas of ventimiglia (NW Italy): the pliocene record of an overfilled messinian incised valley. *Sedimentary Geology, 219*(1–4), 58–76.
Brunet, C., Monié, P., Jolivet, L., & Cadet, J.-P. (2000). Migration of compression and extension in the tyrrhenian sea, insights from 40Ar/39Ar ages on micas along a transect from corsica to tuscany. *Tectonophysics, 321*, 127–155.
Bulard, P. F., Chamagne, B., Dardeau, G., Delteil, J., Gioan, P., Ivaldi, J. P., & Polveche, J. (1975). Sur la genese et les structures de l'arc de nice. *Bulletin De La Société Géologique De France, 7*(6), 939–944.
Butler, R. W., & Mazzoli, S. (2006). *Styles of continental contraction: a review and introduction*. Boulder: Geological Society of America.
Calais, E., Nocquet, J.-M., Jouanne, F., & Tardy, M. (2001). Current strain regime in the Western Alps from continuous global positioning system measurements, 1996–2001. *Geology, 30*, 651–654.
Campani, M., Mancktelow, N., & Courrioux, G. (2014). The 3D interplay between folding and faulting in a syn-orogenic extensional system: the Simplon Fault Zone in the Central Alps (Switzerland and Italy). *Swiss Journal of Geosciences, 107*(2), 251–271.
Campani, M., Mancktelow, N., Seward, D., Rolland, Y., Müller, W., & Guerra, I. (2010). Geochronological evidence for continuous exhumation through the ductile-brittle transition along a crustal-scale low-angle normal fault: simplon fault zone, central Alps. *Tectonics*. https://doi.org/10.1029/2009TC002582
Capponi, G., Crispini, L., Federico, L., Piazza, M., & Fabbri, B. (2009). Late Alpine tectonics in the Ligurian Alps: constraints from the tertiary piedmont basin conglomerates. *Geological Journal, 44*(2), 211–224.
Cardello, G. L., Almqvist, B. S., Hirt, A. M., & Mancktelow, N. S. (2016). Determining the timing of formation of the rawil depression in the Helvetic Alps by palaeomagnetic and structural methods. *Geological Society, 425*(1), 145–168.
Cardello, G. L., & Mancktelow, N. S. (2015). Veining and post-nappe transtensional faulting in the SW Helvetic Alps (Switzerland). *Swiss Journal of Geosciences, 108*(2), 379–400.
Carminati, E., Lustrino, M., & Doglioni, C. (2012). Geodynamic evolution of the central and western mediterranean: tectonics vs. igneous petrology constraints. *Tectonophysics, 579*, 173–192.
Carminati, E., Wortel, M. J. R., Spakman, W., & Sabadini, R. (1998). The role of slab detachment processes in the opening of the westerncentral mediterranean basins: some geological and geophysical evidence. *Earth Planet Sci Let, 160*, 651–665.
Carrapa, B., Bertotti, G., & Wijbrans, J. (2003). Episodic exhumation in the Western Alps. *Geology, 31*, 601–604.
Cawood, A. J., Bond, C. E., Howell, J. A., Butler, R. W. H., & Totake, Y. (2017). LiDAR, UAV or compass-clinometer? Accuracy, coverage and the effects on structural models. *Journal of Structural Geology, 98*, 67–82.
Champagnac, J. D., Sue, C., Delacou, B., Tricart, P., Allanic, C., & Burkhard, M. (2006). Miocene lateral extrusion in the inner western Alps revealed by dynamic fault analysis. *Tectonics*. https://doi.org/10.1029/2004TC001779
Chaumillon, E., Déverchère, J., Rehault, J. P., & Gueguen, E. (1994). Réactivation tectonique et flexure de la marge continentale Ligure (Méditerranée Occidentale). Comptes rendus de l'académie des sciences série 2-mécanique-physique. *Chimie, Sciences De L'univers, Sciences De La Terre, 319*, 675–682.
Clauzon, G., & Rubino, J. L. (1995). Peri-mediterranean pliocene basins are very large scale incised valleys filled by Gilbert-type fan deltas. *Am Assoc Petrol Geol Bull, 79*, 1203–1204.
CloudCompare—Open Source Project. http://www.cloudcompare.org/. Accessed on 1 January 2023.
Collettini, C., Tesei, T., Scuderi, M. M., Carpenter, B. M., & Viti, C. (2019). Beyond Byerlee friction, weak faults and implications for slip behavior. *Earth and Planetary Science Letters, 519*, 245–263.
Collombet, M., Thomas, J. C., Chauvin, A., Tricart, P., Bouillin, J. P., & Gratier, J. P. (2002). Counter-clockwise rotation of the western Alps since the Oligocene: new insights from paleomagnetic data. *Tectonics*. https://doi.org/10.1029/2001TC901016
Crispini, L., Federico, L., Capponi, G., & Spagnolo, C. (2009). Late orogenic transpressional tectonics in the «Ligurian Knot». *Bollettino Della Società Geologica Italiana, 128*(2), 433–441.
Dallagiovanna G, Gaggero L, Seno S, Felletti F, Mosca P, Decarlis A, Pellegrini L, Poggi F, Bottero D, Mancin N, Lupi C, Bonini L, Lualdi A, Maino M, Toscani G. 2011. Note Illustrative della Carta Geologica d'Italia alla scala 1:50.000, foglio 228 Cairo Montenotte. ISPRA - Regione Liguria, Litografia Artistica Cartografica s.r.l. 156 p.
Dallagiovanna, G., Gaggero, L., Maino, M., Seno, S., & Tiepolo, M. (2009). U-Pb zircon ages for post-variscan volcanism in the Ligurian Alps (Northern Italy). *Journal of the Geological Society of London, 166*, 101–114.
Dallagiovanna, G., Maino, M., Mancin, N., Seno, S., & Giacomini, F. (2010). Oligo-Miocene tectonic evolution of the Finalese area (Ligurian Alps, NW Italy). *Rendiconti Online Della Società Geologica Italiana, 10*(1), 39–41.
Davis, G. H., Bump, A. P., García, P. E., & Ahlgren, S. G. (2000). Conjugate riedel deformation band shear zones. *Journal of Structural Geology, 22*(2), 169–190.
de Voogd, B., Nicolich, R., Olivet, J. L., Fanucci, F., Burrus, J., & Mauffret, A. (1991). First deep seismic reflection transect from the Gulf of Lions to Sardinia (ECORS-crop profiles in Western Mediterranean). *American Geophysical Union (AGU), 22*, 265–274. https://doi.org/10.1029/gd022p0265
Decarlis, A., Dallagiovanna, G., Lualdi, A., Maino, M., & Seno, S. (2013). Stratigraphic evolution in the Ligurian Alps between Variscan heritages and the Alpine Tethys opening: a review. *Earth-Science Reviews, 125*, 43–68.
Decarlis, A., & Lualdi, A. (2011). Synrift sedimentation on the northern Tethys margin: an example from the Ligurian Alps (Upper Triassic to Lower Cretaceous, Prepiedmont domain, Italy). *International Journal of Earth Sciences, 100*, 1589–1604.
Decarlis, A., Maino, M., Dallagiovanna, G., Lualdi, A., Masini, E., Seno, S., & Toscani, G. (2014). Salt tectonics in the SW Alps (Italy-France): from rifting to the inversion of the European continental margin in a context of oblique convergence. *Tectonophysics, 636*, 293–314.
Della Porta, G., Nembrini, M., Berra, F., & Vertino, A. (2022). Facies character and skeletal composition of heterozoan carbonates in a high-energy confined embayment (Miocene, Finale Ligure Limestone, NW Italy). *Sedimentary Geology, 438*, 106209.
Delvaux, D., & Sperner, B. (2003). Stress tensor inversion from fault kinematic indicators and focal mechanism data: the TENSOR program. *New Insights into Structural Interpretation and Modelling, 212*, 75–100.
Deng, Q., & Zhang, P. (1984). Research on the geometry of shear fracture zones. *Journal of Geophysical Research: Solid Earth, 89*(B7), 5699–5710.
Dewey, J. F., Helman, M. L., Turco, E., Hutton, D. H. W., & Knott, S. D. (1989). Kinematics of the Western Mediterranean. *Geological Society Special Publication, 45*, 265–283.
Doglioni, C. (1991). A proposal for the kinematic modelling of W-dipping subductions-possible applications to the Tyrrhenian-Apennines system. *Terra Nova, 3*(4), 423–434.
Elter, P., & Pertusati, P. C. (1973). CONSIDERAZIONI SUL LIMITE ALPI-APPENNINO E SULLE SUE RELAZIONI CON L'ARCO DELLE ALPI OCCIDENTALI.
Eva, E., & Solarino, S. (1998). Variations of stress directions in the western Alpine arc. *Geophysical Journal International, 133*, 1–11.
Faccenna, C., Piromallo, C., Crespo-Blanc, A., Jolivet, L., & Rossetti, F. (2004). Lateral slab deformation and the origin of the western Mediterranean arcs. *Tectonics*. https://doi.org/10.1029/2002TC001488
Faulkner, D. R., Mitchell, T. M., Jensen, E., & Cembrano, J. (2011). Scaling of fault damage zones with displacement and the implications for fault growth

processes. *Journal of Geophysical Research: Solid Earth*. https://doi.org/10.1029/2010JB007788
Federico, L., Crispini, L., Vigo, A., & Capponi, G. (2014). Unravelling polyphase brittle tectonics through multi-software fault-slip analysis: the case of the Voltri Unit, Western Alps (Italy). *Journal of Structural Geology, 68*, 175–193.
Federico, L., Maino, M., Capponi, G., & Crispini, L. (2020). Paleo-depth of fossil faults estimated from paleostress state: applications from the Alps and the Apennines (Italy). *Journal of Structural Geology, 140*, 104152. https://doi.org/10.1016/j.jsg.2020.104152
Federico, L., Spagnolo, C., Crispini, L., & Capponi, G. (2009). Fault-slip analysis in the metaophiolites of the Voltri Massif: constraints for the tectonic evolution at the Alps/Apennine boundary. *Geological Journal, 44*(2), 225–240. https://doi.org/10.1002/gj.1139
Foeken, J. P. T., Dunai, T. J., Bertotti, G., & Andriessen, P. A. M. (2003). Late Miocene to present exhumation in the Ligurian Alps (southwest Alps) with evidence for accelerated denudation during the Messinian salinity crisis. *Geology, 31*(9), 797–800.
Ford, M., Duchêne, S., Gasquet, D., & Vanderhaeghe, O. (2006). Two-phase orogenic convergence in the external and internal SW Alps. *Journal of the Geological Society of London, 161*, 815–826.
Fossen, H., Cavalcante, G. C. G., Pinheiro, R. V. L., & Archanjo, C. J. (2019). Deformation–progressive or multiphase? *Journal of Structural Geology, 125*, 82–99.
Gattacceca, J., Deino, A., Rizzo, R., Jones, D. S., Henry, B., Beaudoin, B., & Vadeboin, F. (2007). Miocene rotation of Sardinia: new paleomagnetic and geochronological constraints and geodynamic implications. *Earth and Planetary Science Letters, 258*(3–4), 359–377. https://doi.org/10.1016/j.epsl.2007.02.003
Gelati, R., Gnaccolini, M., & Petrizzo, M. R. (1998). Synsedimentary tectonics and sedimentation in the Tertiary Piedmont Basin, northwestern Italy. *Rivista Italiana Di Paleontologia e Stratigrafia, 104*(2), 193–213.
Gèze B, Lanteaume M, 1963. Carte géologique de Menton-Nice, Editions BRGM.
Giglia, G., Capponi, G., Crispini, L., & Piazza, M. (1996). Dynamics and seismotectonics of the West-Alpine arc. *Tectonophysics, 267*(1–4), 143–175.
Goffé, B., & Bousquet, R. (2004). Metamorphic structure of the Alps: Western and Ligurian Alps. *Nature, 387*, 586–589.
Handy, M. R., Schmid, S. M., Bousquet, R., Kissling, E., & Bernoulli, D. (2010). Reconciling plate-tectonic reconstructions of Alpine Tethys with the geological–geophysical record of spreading and subduction in the Alps. *Earth-Science Reviews, 102*(3–4), 121–158.
Handy, M. R., Schmid, S. M., Paffrath, M., & Friederich, W. (2021). Orogenic lithosphere and slabs in the greater Alpine area–interpretations based on teleseismic P-wave tomography. *Solid Earth, 12*(11), 2633–2669.
Inama, R., Menegoni, N., & Perotti, C. (2020). Syndepositional fractures and architecture of the lastoni di formin carbonate platform: insights from virtual outcrop models and field studies. *Marine and Petroleum Geology, 121*, 104606.
Jolivet, L., & Faccenna, C. (2000). Mediterranean extension and the Africa-Eurasia collision. *Tectonics, 19*, 1095–1106.
Kästle, E. D., Rosenberg, C., Boschi, L., Bellahsen, N., Meier, T., & El-Sharkawy, A. (2020). Slab break-offs in the Alpine subduction zone. *International Journal of Earth Sciences, 109*, 587–603.
Katz, Y., Weinberger, R., & Aydin, A. (2004). Geometry and kinematic evolution of Riedel shear structures, Capitol Reef National Park Utah. *Journal of Structural Geology, 26*(3), 491–501.
Larroque, C., de Lépinay, B. M., & Migeon, S. (2011). Morphotectonic and fault–earthquake relationships along the northern Ligurian margin (western Mediterranean) based on high resolution, multibeam bathymetry and multichannel seismic-reflection profiles. *Marine Geophysical Research, 32*(1–2), 163–179.
Larroque, C., Delouis, B., Godel, B., & Nocquet, J. M. (2009). Active deformation at the southwestern Alps-Ligurian basin junction (France–Italy boundary): evidence for recent change from compression to extension in the Argentera massif. *Tectonophysics, 467*(1–4), 22–34.
Laubscher, H. P., Biella, G. C., Cassinis, R., Gelati, R., Lozej, A., Scarascia, S., & Tabacco, I. (1992). The collisional knot in Liguria. *Geologische Rundschau, 81*, 275–289.
Le Breton, E., Brune, S., Ustaszewski, K., Zahirovic, S., Seton, M., & Müller, R. D. (2021). Kinematics and extent of the Piemont-Liguria Basin–implications for subduction processes in the Alps. *Solid Earth, 12*(4), 885–913.
Li, H., Pan, J., Lin, A., Sun, Z., Liu, D., Zhang, J., & Gong, Z. (2016). Coseismic surface ruptures associated with the 2014 Mw 69 yutian earthquake on the Altyn Tagh fault, Tibetan Plateau Coseismic surface ruptures associated with the 2014 Mw 69 yutian earthquake on the ATF. *Bulletin of the Seismological Society of America, 106*(2), 595–608.
Maffione, M., Speranza, F., Faccenna, C., Cascella, A., Vignaroli, G., & Sagnotti, L. (2008). A synchronous Alpine and Corsica-Sardinia rotation. *Journal of Geophysical Research: Solid Earth, 113*, B03104. https://doi.org/10.1029/2007JB005214
Maino, M., Adamuszek, M., Schenker, F. L., Seno, S., & Dabrowski, M. (2021). Sheath fold development around deformable inclusions: Integration of field-analysis (Cima Lunga unit, Central Alps) and 3D numerical models. *Journal of Structural Geology, 144*, 104255.
Maino, M., Bonini, L., Dallagiovanna, G., & Seno, S. (2015a). Large sheath folds in the Briançonnais of the Ligurian Alps reconstructed by analysis of minor structures and stratigraphic mapping. *Journal of Maps, 11*(1), 157–167.
Maino, M., Casini, L., Boschi, C., Di Giulio, A., Setti, M., & Seno, S. (2020). Time-dependent heat budget of a thrust from geological records and numerical experiments. *Journal of Geophysical Research: Solid Earth*. https://doi.org/10.1029/2019JB018940
Maino, M., Casini, L., Ceriani, A., Decarlis, A., Di Giulio, A., Seno, S., & Stuart, F. M. (2015b). Dating shallow thrusts with zircon (U-Th)/He thermochronometry—the shear heating connection. *Geology, 43*(6), 495–498.
Maino, M., Dallagiovanna, G., Dobson, K. J., Gaggero, L., Persano, C., Seno, S., & Stuart, F. M. (2012). Testing models of orogen exhumation using zircon (U–Th)/He thermochronology: Insight from the Ligurian Alps, Northern Italy. *Tectonophysics, 560–561*, 84–93. https://doi.org/10.1016/j.tecto.2012.06.045
Maino, M., Decarlis, A., Felletti, F., & Seno, S. (2013). Tectono-sedimentary evolution of the Tertiary Piedmont Basin (NW Italy) within the Oligo-Miocene central Mediterranean geodynamics. *Tectonics, 32*(3), 593–619. https://doi.org/10.1002/tect.20047
Maino, M., Gaggero, L., Langone, A., Seno, S., & Fanning, M. (2019). Cambro-Silurian magmatisms at the northern Gondwana margin (Penninic basement of the Ligurian Alps). *Geoscience Frontiers, 10*(1), 315–330. https://doi.org/10.1016/j.gsf.2018.01.003
Maino, M., & Seno, S. (2016). The thrust zone of the Ligurian Penninic basal contact (Monte Fronté, Ligurian Alps, Italy). *Journal of Maps, 12*(sup1), 341–351.
Malinverno, A., & Ryan, W. B. (1986). Extension in the Tyrrhenian Sea and shortening in the Apennines as result of arc migration driven by sinking of the lithosphere. *Tectonics, 5*(2), 227–245.
Malusà, M. G., Polino, R., & Zattin, M. (2009). Strain partitioning in the axial NW Alps since the Oligocene. *Tectonics*. https://doi.org/10.1029/2008TC002370
Mancktelow, N. S. (1992). Neogene lateral extension during convergence in the Central Alps: evidence from interrelated faulting and backfolding around the Simplonpass (Switzerland). *Tectonophysics, 215*(3–4), 295–317.
Marini M. (2000). Il Pliocene Ligure a Taggia (Imperia, Alpi Marittime liguri) stratigrafia fisica ed evoluzione sedimentaria. Bollettino della Società Geologica Italiana, 119(2), 423–443.
Marrett, R., & Allmendinger, R. W. (1990). Kinematic analysis of fault-slip data. *Journal of Structural Geology, 12*(8), 973–986.
Marrett, R., & Peacock, D. C. (1999). Strain and stress. *Journal of Structural Geology, 21*(8–9), 1057–1063.
Marroni, M., Meneghini, F., Pandolfi, L., Noah, H., & Edoardo, L. (2019). The ottone-levanto line of Eastern liguria (Italy) uncovered: a late eocene-early oligocene snapshot of northern apennine geodynamics at the alps/apennines junction. *Episodes, 42*(2), 107–118.
Marroni, M., Pandolfi, L., Onuzi, K., Palandri, S., & Xhomo, A. (2009). Ophiolite-bearing vermoshi flysch (albanian alps, northern albania): elements for its correlation in the frame of dinaric-hellenic belt. *Ofioliti, 34*(2), 95–108.
Marroni, M., & Treves, B. (1998). Hidden terranes in the Northern Apennines, Italy: a record of late cretaceous-oligocene transpressional tectonics. *The Journal of Geology, 106*(2), 149–162.
McCaffrey, K. J. W., Jones, R. R., Holdsworth, R. E., Wilson, R. W., Clegg, P., Imber, J., & Trinks, I. (2005). Unlocking the spatial dimension: digital

technologies and the future of geoscience fieldwork. *Journal of the Geological Society, 162*(6), 927–938.
Menegoni, N., Giordan, D., Perotti, C., & Tannant, D. D. (2019). Detection and geometric characterization of rock mass discontinuities using a 3D high-resolution digital outcrop model generated from RPAS imagery–ormea rock slope, Italy. *Engineering Geology, 252*, 145–163.
Menegoni, N., Giordan, D., & Perotti, C. (2020). Reliability and uncertainties of the analysis of an unstable rock slope performed on RPAS digital outcrop models: The case of the gallivaggio landslide (Western Alps, Italy). Remote Sensing, 12(10), 1635.
Menegoni, N., Inama, R., Crozi, M., & Perotti, C. (2022a). Early deformation structures connected to the progradation of a carbonate platform: the case of the nuvolau cassian platform (dolomites-Italy). *Marine and Petroleum Geology, 138*, 105574.
Menegoni, N., Inama, R., Panara, Y., Crozi, M., & Perotti, C. (2022b). Relations between fault and fracture network affecting the lastoni di formin carbonate platform (Italian Dolomites) and its deformation history. *Geosciences, 12*(12), 451.
Menegoni, N., Meisina, C., Perotti, C., & Crozi, M. (2018). Analysis by UAV digital photogrammetry of folds and related fractures in the monte antola flysch formation (ponte organasco, Italy). *Geosciences, 8*(8), 299.
Miletto, M., & Polino, R. (1992). A gravity model of the crust beneath the Tertiary Piemonte Basin (NorthWestern Italy). Tectonophysics, 212(3-4), 243-256.
Molli, G., Crispini, L., Malusà, M., Mosca, P., Piana, F., & Federico, L. (2010). Geology of the Western Alps-Northern Apennine junction area: a regional review. Eds Marco Beltrando, Angelo Peccerillo, Massimo Mattei, Sandro Conticelli, and Carlo Doglioni Journal of the Virtual Explorer, 36(3).
Morelli, E., Martorelli, E., Casalbore, D., & Chiocci, F. L. (2022). Morpho-stratigraphic evolution of a tectonically controlled canyon-channel system in the Gioia Basin (Southern Tyrrhenian Sea). *Marine Geology, 451*, 106881.
Mosca, P., Polino, R., Rogledi, S., & Rossi, M. (2010). New data for the kinematic interpretation of the alps-apennines junction (Northwestern Italy). *International Journal of Earth Sciences, 99*(4), 833–849.
Mueller, P., Maino, M., & Seno, S. (2020). Progressive deformation patterns from an accretionary prism (Helminthoid Flysch, Ligurian Alps, Italy). *Geosciences*. https://doi.org/10.3390/geosciences10010026
Mueller, P., Tamburelli, S., Menegoni, N., Perozzo, M., Amadori, C., Crispini, L., & Maino, M. (2023). Concurrence of load-and-flame structures, balls-and-pillows, clastic injectites and shear deformation bands as indicator of seismicity in mixed siliciclastic-carbonate successions (Finale Ligure Basin Italy). *Marine and Petroleum Geology*. https://doi.org/10.1016/j.marpetgeo.2023.106345
Panara, Y., Khanna, P., Chandra, V., Finkbeiner, T., & Vahrenkamp, V. (2022a). 3D digital outcrop model-based fracture network analysis of reservoir outcrop analogue, upper jubaila formation, Saudi Arabia. *83rd EAGE Annu Conf Exhib*. https://doi.org/10.3997/2214-4609.202210861
Panara, Y., Menegoni, N., Carboni, F., & Inama, R. (2022b). 3D digital outcrop model-based analysis of fracture network along the seismogenic Mt. vettore fault system (Central Italy): the importance of inherited fractures. *Journal of Structural Geology, 161*, 104654.
Patacca, E., Sartori, R., & Scandone, P. (1990). Tyrrhenian basin and apenninic arcs: kinematic relations since late tortonian times. *Memorie Della Società Geologica Italiana, 45*, 425–451.
Peppa, M. V., Hall, J., Goodyear, J., & Mills, J. P. (2019). Photogrammetric assessment and comparison of DJI phantom 4 pro and phantom 4 RTK small unmanned aircraft systems. ISPRS Geospatial Week. https://doi.org/10.5194/isprs-archives-XLII-2-W13-503-2019
Perrone, G., Cadoppi, P., Tallone, S., & Balestro, G. (2011). Post-collisional tectonics in the northern cottian alps (Italian western alps). *International Journal of Earth Sciences, 100*, 1349–1373.
Piana, F., Tallone, S., Cavagna, S., & Conti, A. (2006). Thrusting and faulting in metamorphic and sedimentary units of ligurian alps: an example of integrated field work and geochemical analyses. *International Journal of Earth Sciences, 95*(3), 413–430.
Platt, J. P., Behrmann, J. H., Cunningham, P. C., Dewey, J. F., Helman, M., Parish, M., & Western, P. J. (1989). Kinematics of the alpine arc and the motion history of adria. *Nature, 337*(6203), 158–161.
Pleuger, J., Mancktelow, N., Zwingmann, H., & Manser, M. (2012). K-Ar dating of synkinematic clay gouges from neoalpine faults of the central, Western and Eastern alps. *Tectonophysics, 550*, 1–16.
Réhault, J. P., Honthaas, C., Guennoc, P., Bellon, H., Ruffet, G., Cotten, J., & Maury, R. C. (2012). Offshore oligo-miocene volcanic fields within the corsica-liguria basin: magmatic diversity and slab evolution in the western mediterranean sea. *Journal of Geodynamics, 58*, 73–95.
Ricou, L. E., & Siddans, A. W. B. (1986). Continent-continent collision: himalayan-alpine belt. *Geological Society, 19*, 229–244.
Ring, U., Fassoulas, C., Uysal, I. T., Bolhar, R., Tong, K., & Todd, A. (2022). Nappe Imbrication Within the phyllite-quartzite unit of West Crete: Implications for sustained high-pressure metamorphism in the hellenide subduction orogen, Greece. *Tectonics*. https://doi.org/10.1029/2022TC007430
Ring, U., & Gerdes, A. (2016). Kinematics of the alpenrhein-bodensee graben system in the central alps: oligocene/miocene transtension due to formation of the Western Alps arc. *Tectonics, 35*, 1367–1391. https://doi.org/10.1002/2015TC004085
Rollet, N., Déverchère, J., Beslier, M. O., Guennoc, P., Réhault, J. P., Sosson, M., & Truffert, C. (2002). Back arc extension, tectonic inheritance, and volcanism in the ligurian sea, Western mediterranean. *Tectonics, 21*(3), 66–23. https://doi.org/10.1029/2001TC900027
Rosenbaum, G., & Lister, G. S. (2004). Formation of arcuate orogenic belts in the western mediterranean region. *Orogenic Curvature: Integrating Paleomagnetic and Structural Analyses, 383*, 41–56.
Rosenbaum, G., Lister, G. S., & Duboz, C. (2002). Reconstruction of the tectonic evolution of the western mediterranean since the oligocene. *Journal of the Virtual Explorer, 8*, 107–126.
Rossetti, F., Faccenna, C., Goffé, B., Monié, P., Argentieri, A., Funiciello, R., & Mattei, M. (2001). Alpine structural and metamorphic signature of the sila piccola massif nappe stack (Calabria, Italy): Insights for the tectonic evolution of the Calabrian Arc. *Tectonics, 20*, 112–133. https://doi.org/10.1029/2000TC900027
Savage, H. M., & Brodsky, E. E. (2011). Collateral damage: evolution with displacement of fracture distribution and secondary fault strands in fault damage zones. *Journal of Geophysical Research: Solid Earth*. https://doi.org/10.1029/2010JB007665
Schmid, S. M., Fügenschuh, B., Kissling, E., & Schuster, R. (2004). Tectonic map and overall architecture of the alpine orogen. *Eclogae Geologicae Helvetiae, 97*(1), 93–117.
Schmid, S. M., & Kissling, E. (2000). The arc of the western alps in the light of geophysical data on deep crustal structure. *Tectonics, 19*(1), 62–85.
Schmid, S. M., Pfiffner, O. A., Froitzheim, N., Schönborn, G., & Kissling, E. (1996). Geophysical–geological transect and tectonic evolution of the swiss-Italian alps. *Tectonics, 15*(5), 1036–1064.
Schmid, S. M., Kissling, E., Diehl, T., van Hinsbergen, D. J., & Molli, G. (2017). Ivrea mantle wedge, arc of the Western Alps, and kinematic evolution of the Alps–Apennines orogenic system. Swiss Journal of Geosciences, 110, 581-612.
Seno, S., Dallagiovanna, G., & Vanossi, M. (2005). A kinematic evolutionary model for the penninic sector of the central ligurian alps. *International Journal of Earth Sciences, 94*, 114–129.
Séranne, M. (1999). The Gulf of Lion continental margin (NW Mediterranean) revisited by IBS: an overview. *Spec Publ Geol Soc*. https://doi.org/10.1144/GSL.SP.1999.156.01.03
Servizio Geologico d'Italia. (1971). *Carta geologica d'Italia alla scala 1:100.000, F. 92–93 albenga-savona*. Roma: ISPRA.
Siravo, G., Speranza, F., & Mattei, M. (2023). Paleomagnetic evidence for pre-21 Ma independent drift of South Sardinia from North Sardinia-Corsica:"Greater Iberia" vs. Europe. *Tectonics*. https://doi.org/10.1029/2022TC007705
Soulet, Q., Migeon, S., Gorini, C., Rubino, J. L., Raisson, F., & Bourges, P. (2016). Erosional versus aggradational canyons along a tectonically-active margin: the northeastern ligurian margin (western Mediterranean Sea). *Marine Geology, 382*, 17–36.
Spagnolo, C., Crispini, L., & Capponi, G. (2007). Late structural evolution in an accretionary wedge: insights from the Voltri Massif (Ligurian Alps, Italy). Geodinamica Acta, 20(1-2), 21-35.
Speranza, F., Villa, I. M., Sagnotti, L., Florindo, F., Cosentino, D., Cipollari, P., & Mattei, M. (2002). Age of the corsica-sardinia rotation and liguro-provençal

basin spreading: new paleomagnetic and Ar/Ar evidence. *Tectonophysics, 347*(4), 231–251.
Stott, E., Williams, R. D., & Hoey, T. B. (2020). Ground control point distribution for accurate kilometre-scale topographic mapping using an RTK-GNSS unmanned aerial vehicle and SfM photogrammetry. *Drones, 4*(3), 55.
Štroner, M., Urban, R., Reindl, T., Seidl, J., & Brouček, J. (2020). Evaluation of the georeferencing accuracy of a photogrammetric model using a quadrocopter with onboard GNSS RTK. *Sensors, 20*(8), 2318.
Sue, C., & Tricart, P. (2003). Neogene to ongoing normal faulting in the inner western alps: a major evolution of the late alpine tectonics. *Tectonics*. https://doi.org/10.1029/2002TC001426
Taddia, Y., González-García, L., Zambello, E., & Pellegrinelli, A. (2020). Quality assessment of photogrammetric models for façade and building reconstruction using DJI phantom 4 RTK. *Remote Sensing, 12*(19), 3144.
Taddia, Y., Stecchi, F., & Pellegrinelli, A. (2019). Using DJI phantom 4 RTK drone for topographic mapping of coastal areas. *The International Archives of Photogrammetry, Remote Sensing and Spatial Information Sciences, 42*, 625–630.
Taddia, Y., Stecchi, F., & Pellegrinelli, A. (2020). Coastal mapping using DJI Phantom 4 RTK in post-processing kinematic mode. *Drones, 4*(2), 9.
Tarasewicz, J. P., Woodcock, N. H., & Dickson, J. A. D. (2005). Carbonate dilation breccias: examples from the damage zone to the Dent Fault, northwest England. *Geological Society of America Bulletin, 117*(5–6), 736–745.
Tavarnelli, E., Butler, R. W. H., Decandia, F. A., Calamita, F., Grasso, M., Alvarez, W., & Renda, P. (2004). Implications of fault reactivation and structural inheritance in the Cenozoic tectonic evolution of Italy. *Special Volume Geological Society of Italy, 186*, 209–222.
Taylor, M., Yin, A., Ryerson, F. J., Kapp, P., & Ding, L. (2003). Conjugate strike-slip faulting along the Bangong-Nujiang suture zone accommodates coeval east-west extension and north-south shortening in the interior of the Tibetan Plateau. *Tectonics*. https://doi.org/10.1029/2002TC001361
Thiele, S. T., Bnoulkacem, Z., Lorenz, S., Bordenave, A., Menegoni, N., Madriz, Y., Dujoncquoy, E., Gloaguen, R., & Kenter, J. (2022). Mineralogical mapping with accurately corrected shortwave infrared hyperspectral data acquired obliquely from UAVs. *Remote Sensing, 14*, 5. https://doi.org/10.3390/rs14010005
Thomas, J. C., Claudel, M. E., Collombet, M., Chauvin, A., & Dumont, T. (1999). First paleomagnetic data from the sedimentary cover of the french penninic alps: evidence for tertiary counterclockwise rotations in the Western Alps, Earth Planet. *Sci Lett, 171*, 561–574.
Trümpy, R. (1960). Paleotectonic evolution of the central and western Alps. Bulletin of the Geological Society of America, 71, 843–908.
Twiss, R. J., & Unruh, J. R. (1998). Analysis of fault slip inversions: do they constrain stress or strain rate? *Journal of Geophysical Research: Solid Earth, 103*(B6), 12205–12222.
van Hinsbergen, D. J. J., Vissers, R. L. M., & Spakman, W. (2014). Origin and consequences of western mediterranean subduction, rollback, and slab segmentation. *Tectonics, 33*, 393–419. https://doi.org/10.1002/tect.20125
Vanik, N., Shaikh, M. A., Mukherjee, S., Maurya, D. M., & Chamyal, L. S. (2018). Post-Deccan trap stress reorientation under transpression: evidence from fault slip analyses from SW Saurashtra, western India. *Journal of Geodynamics, 121*, 9–19.
Vanossi M. 1991. Guide Geologiche Regionali - Alpi Liguri (a cura della Societa` Geologica Italiana), BEMA Ed., 293 pp.
Vanossi, M., Corte Sogno, L., Galbiati, B., Messiga, B., Piccardo, G., & Vannucci, R. (1984). Geologia delle Alpi Liguri: dati, problemi, ipotesi. *Memorie Della Società Geologica Italiana, 28*, 5–75.
Vanossi, M., Perotti, C. R., & Seno, S. (1994). The maritime alps arc in the ligurian and tyrrhenian systems. *Tectonophysics, 230*(1–2), 75–89. https://doi.org/10.1016/0040-1951(94)90147-3
Vignaroli, G., Faccenna, C., Jolivet, L., Piromallo, C., & Rossetti, F. (2008). Subduction polarity reversal at the junction between the Western Alps and the Northern Apennines, Italy. *Tectonophysics, 450*, 34–50.
Vignaroli, G., Rossetti, F., Rubatto, D., Theye, T., Lisker, F., & Phillips, D. (2010). Pressure-temperature-deformation-time (P-T-d-t) exhumation history of the voltri massif hp complex, ligurian alps, Italy. *Tectonics*. https://doi.org/10.1029/2009TC002621
Westoby, M. J., Brasington, J., Glasser, N. F., Hambrey, M. J., & Reynolds, J. M. (2012). 'Structure-from-Motion' photogrammetry: a low-cost, effective tool for geoscience applications. *Geomorphology, 179*, 300–314.
Woodcock, N. H., Dickson, J. A. D., & Tarasewicz, J. P. T. (2007). Transient permeability and reseal hardening in fault zones: evidence from dilation breccia textures. *Geological Society, 270*(1), 43–53.
Woodcock, N. H., & Mort, K. (2008). Classification of fault breccias and related fault rocks. *Geological Magazine, 145*(3), 435–440.

Publisher's Note